Cell Tissue Res (1997) 288:449–469

Cell & Tissue Research

Ultrastructural features of tyrosine-hydroxylase-immunoreactive afferents and their targets in the rat amygdala

E. Asan

Department of Anatomy, University of Würzburg, Koellikerstraße 6, D-97070 Würzburg, Germany

Received: 23 May 1996 / Accepted: 24 October 1996

Abstract. Interrelations of tyrosine-hydroxylase-immunoreactive afferent fibres with neuronal elements were studied in central, basal and intercalated nuclei of the rat amygdaloid complex. Comparison with dopamine-β-hydroxylase-immunoreacted and phenylethanolamine-*N*-methyltransferase-immunoreacted parallel sections indicated that the tyrosine-hydroxylase immunoreaction labelled preferentially dopaminergic axons. At the electron-microscopic level, the majority of tyrosine-hydroxylase-immunoreactive axons possessed small boutons containing small clear vesicles and contacting dendrites, spines or somata of amygdala neurons, forming mostly symmetric synapses. They were often directly apposed to or in the vicinity of unlabelled terminals synapsing on the same structure. Synaptic density was highest in the central lateral part of the central nucleus. In the central and basal nuclei labelled axons synapsed preferentially on small dendrites and dendritic spines, and on somata of a few neurons. A detailed study of the neuronal ultrastructure showed that innervated somata possessed the differential characteristics displayed by the predominant neuron types in the medial and central lateral central nucleus and resembled the typical projection neurons in the basal nuclei. In the paracapsular intercalated cell groups the majority of neurons possessed intense perisomatic innervation by immunoreactive terminals. The results suggest that tyrosine-hydroxylase-immunoreactive, predominantly dopaminergic amygdaloid afferent fibres preferentially modulate the effect of extrinsic inputs into neurons of the central and basal nuclei, while a nonselective regulation is exerted upon the output of paracapsular intercalated neurons. It is suggested that this innervation pattern may be important for the coordinated integration of extrinsic and intraamygdaloid connections and thus for balanced output of the structure.

Key words: Neuronal ultrastructure – Catecholamines – Dopamine – Immunocytochemistry – Connections – Quantitation – Rat (Wistar)

Introduction

Studies in patients with bilateral amygdala damage have documented that this brain area is essential for the recognition of emotion in facial expressions (Adolphs et al. 1994) and participates in the perception of social signals (Allman and Brothers 1994; Tovée 1995). The findings indicate that in humans, as in experimental animals from rodents to monkeys, the amygdala plays a key role in processes subserving social communication. It is important for the formation of emotional memory and the expression of emotional behaviour, particularly involving fear (LeDoux 1994) as well as for associative learning and attentional processes (Gallagher and Holland 1994). It has been suggested that dysfunctions in neural systems connected with the amygdala could be responsible for, for instance, the interactional problems typical for autism or for the distorted perception of social signals and the inappropriate fear responses seen in paranoid delusional states (Allman and Brothers 1994).

In this context, attention has been drawn to the catecholaminergic (CA) innervation of the amygdala. In particular, the dopaminergic (DA) amygdala innervation has been proposed as a possible candidate for mediating delusional, fear-related processes (Fibiger 1991). Additionally, both the DA and the noradrenergic (NA) innervation have been shown to be influential in amygdaloid interface functions between cognitive and autonomic processes. Thus, noradrenalin and dopamine injections into the central amygdaloid nucleus (CN) were found to alter the rate of gastric ulcer formation in rats subjected to stressful experiences (Glavin et al. 1991).

This paper is dedicated to Professor Andreas Oksche on the occasion of his 70th birthday, in recognition of outstanding contributions to neuroscience and to the internationalisation of science

Tel.: (931) 312703; Fax: (931) 15988

This study was supported by the Deutsche Forschungsgemeinschaft, grants As 89/1–2

In the rat, as in other species including the monkey, the amygdaloid complex possesses a dense CA innervation (Sadikot and Parent 1990; Fallon and Ciofi 1992; Asan 1993; Freedman and Cassell 1994), targeted primarily at the CN and basal nuclei (basal complex, BC), and, in the case of the DA afferent fibres, at intercalated amygdaloid cell groups (I). These nuclei have different tasks in learning about, remembering and reacting to fear (LeDoux 1994). They differ greatly in their cyto- and chemoarchitecture as well as in their connections (e.g. DeOlmos et al. 1985; Price et al. 1987; Alheid et al. 1995). In view of the differential characteristics of the amygdaloid nuclei, it is likely that each type of CA innervation subserves distinct functions in each of them. In fact, in the rat, differing biochemical and pharmacological characteristics have been documented for the DA afferent fibres serving the different nuclei, indicating a focal role of DA in modulating their output and suggesting that changes in this innervation may be substantial during the action of antipsychotic drugs (Kilts et al. 1988).

In spite of the possible functional significance of the amygdaloid CA innervation, little information is available concerning its mode of action. A necessary basis for investigations into this question is a detailed knowledge of the morphology of the interactions between the identified afferent fibres and their target structures. Therefore, in the present investigation, interrelationships between afferent fibres immunoreactive (ir) for the rate-limiting enzyme in catecholamine biosynthesis, tyrosine-hydroxylase (TH) and neurons in the CN, BC and paracapsular Is were studied at the ultrastructural level. Dopamine β-hydroxylase (DBH)- and phenylethanolamine *N*-methyltransferase (PNMT) immunoreactions on parallel sections served to assess the extent to which NA and adrenergic (A) afferent fibres in the amygdala were labelled by the TH immunoreaction. Additionally, characteristic ultrastructural features of neurons in the different nuclei were studied and documented in order to be able to classify and identify innervated neurons.

Materials and methods

Tissue treatment

The brains of 13 untreated adult male Wistar rats were used in this study. All animals were perfused under deep pentobarbital anaesthesia via the ascending aorta. Following a short vascular rinse with 0.1 M phosphate-buffered saline pH 7.2 (PBS), 11 brains were fixed with 4% paraformaldehyde (PFA) at variable pH (Berod et al. 1981; modified by Liposits et al. 1986). The brains were perfused for 10 min with the low-pH component (pH 6.5), followed by a perfusion of 20 min with the alkaline component (pH 10.5) to which 0.02% glutaraldehyde (GA) had been added. After fixation, the brains were removed from the skulls and cut in half by a midline sagittal cut. Frontal blocks 5 mm in thickness of the amygdaloid region were dissected and postfixed in the alkaline component of the fixative without GA for either 1–3 h at room temperature or overnight at 4° C. Following washing in PBS, some blocks were successively infiltrated with 10% and 20% sucrose in PBS, frozen in liquid-nitrogen-cooled propane and stored at –70° C. Some blocks were not frozen; the rest was frozen and processed as described below without storage.

A comparison of the different methods showed that freezing and, more so, storage was somewhat detrimental to the ultrastructural preservation. However, the initial quality of the fixation of the tissue was more relevant for these experiments, and freezing of the tissue resulted in a more intense immunocytochemical signal. For sectioning, frozen tissue blocks were slowly thawed and put into PBS. Frontal sections of all tissue blocks were prepared on a Vibratome Model 1000 at a thickness of 40–50 μm. Sections were collected in several series per block. One series was immediately mounted from destilled H_2O and stained with cresyl violet; the others were washed extensively in PBS before being subjected to immunocytochemical treatment (see below).

For electron-microscopic analyses of neurons in the different amygdaloid nuclei (see below), the brains of two animals that had been perfused and fixed using fixative with high concentrations of GA according to the method of Erselius and Wree (1991) were sectioned. Fixed brains were washed extensively in PBS, the amygdaloid region was dissected, and 200-μm-thick Vibratome sections were cut. Further treatment and preparation of ultrathin sections was as described for the sections of tissue fixed at variable pH (see below).

Immunocytochemistry

Free floating incubations of one series of Vibratome sections were done in monoclonal mouse anti-TH antiserum (Boehringer, Mannheim, Germany) diluted 1:50 in PBS with 0.25% lambda-carrageenan (Type IV; Sigma, Deisenhofen, Germany) and 0.04% Triton X-100 (Sigma). A second series of sections was incubated in polyclonal rabbit anti-DBH antiserum (Eugene Tech. Int., USA) diluted 1:500 in the same buffer. Other series were incubated with anti-TH or anti-DBH antiserum in the same buffer but with 0.5% Triton X-100 for preparations for comparative light microscopy (LM). Additional sections were incubated in polyclonal rabbit anti-PNMT (Eugene Tech Int.) for electron microscopy (EM) and LM. All sections were incubated for 48–72 h at 4° C, washed in PBS, transferred to biotinylated rabbit anti-mouse or swine anti-rabbit IgG (DAKO, Hamburg, Germany; 1:300 for 3 h at room temperature or 1:500 overnight at 4° C), washed again in PBS, incubated in an avidin-biotin–horseradish-peroxidase complex (DAKO) in PBS for 2.5 h and washed again in PBS.

Visualization was carried out using the glucose-oxidase-diaminobenzidine (DAB) method described by Zaborsky and Heimer (1989). Immunoreaction product development was checked by LM and stopped by repeated washes in PBS when the maximum specific labelling possible was achieved. Immunolabelling on the majority of sections was intensified using either a nickel (NiDAB; Zaborsky and Heimer 1989) or a silver–gold intensification of the DAB reaction product (SGI–DAB; Liposits et al. 1986). LM preparations were mounted onto slides pretreated with chrome-alum–gelatine. Following drying, a number of TH-labelled sections were counterstained with cresyl violet. All LM sections were dehydrated in a graded ethanol series and mounted in DePex (Serva, Heidelberg, Germany) from xylene.

Treatment for electron microscopy

DAB-reacted sections with and without intensification, some serial sections which had not been immunocytochemically reacted, and the thick Vibratome sections of the GA-fixed brains were washed in PBS, postfixed in 1% OsO4 in PBS for 1 h, washed again in PBS, dehydrated in a graded–ethanol series and embedded in Durcupan (Fluka, Neu-Ulm, Germany) between two microscopic slides. After hardening of the resin, the top slides were removed, and the sections were observed by LM. Amygdaloid nuclei were defined by comparison of the embedded sections with the series of cresyl-violet-stained sections of the same tis-

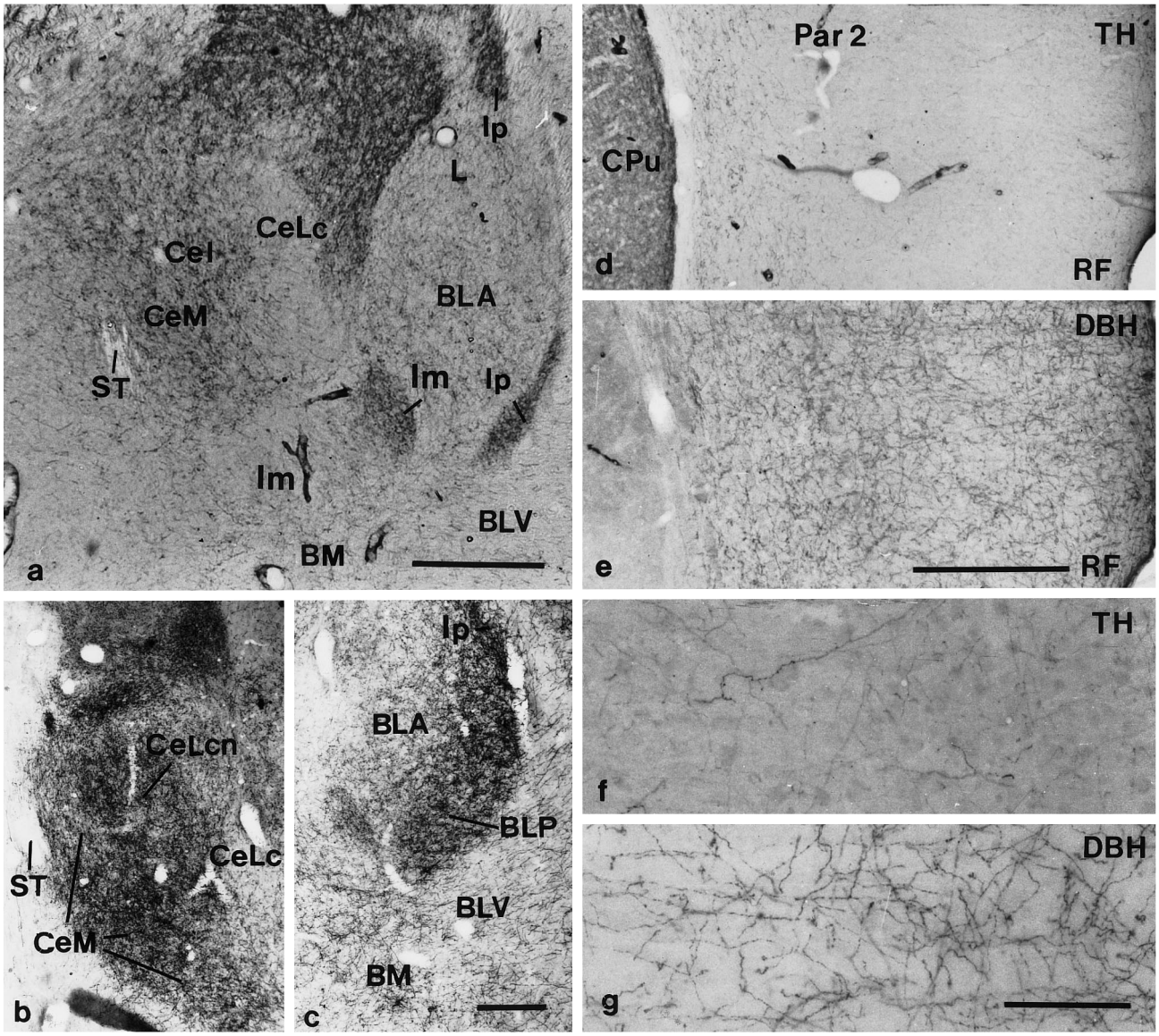

Fig. 1. a Low-magnification microphotograph of a TH-immunoreacted coronal section of part of the rat amygdala at interaural level (IAL) ca. 6.8. **b**, **c** TH immunoreaction in the central nucleus (**b**) and the basal complex nuclei (**c**) at an IAL of ca. 6.2. **d** TH-ir fibres in and ventral to area 2 of the parietal cortex (*Par 2*) adjacent to the amygdala shown in **a**. **e** DBH-ir fibres in the same area in a parallel section. **f**, **g** Higher magnifications of cortical layers II–IV from the *upper right regions* of **d** and **e**. Note that the number of DBH-ir fibres is high in these cortical layers while TH-ir fibres are scarce. *BLA*, Anterior basolateral nucleus; *BLP*, posterior basolateral nucleus; *BLV*, ventral basolateral nucleus; *BM*, basomedial nucleus; *CeI*, intermediate central nucleus; *CeLc*, lateral capsular central nucleus; *CeLcn*, central lateral central nucleus; *CeM*, medial central nucleus; *CPu*, caudate putamen; *Im*, main intercalated cell groups; *Ip*, paracapsular intercalated cell groups; *L*, lateral nucleus; *RF*, rhinal fissure; *ST*, stria terminalis. *Bars:* 500 μm in **a** and **e** (same magnification in **d**); 200 μm in **c** (same magnification in **b**); 100 μg in **g** (same magnification in **f**)

sue block. Small areas situated within or including the different nuclei were cut out from GA-fixed sections and from TH-immunoreacted sections of eight different amygdalae for the CN and the BC and of five amygdalae for Is (see below) and were reembedded upon empty Durcupan blocks. Ultrathin sections (Fig. 1) were cut, mounted on 200 mesh-thin-bar nickel grids (Plano, Marburg, Germany), lightly contrasted with uranyl acetate and lead citrate (Reynolds 1963) and observed in a Zeiss EM 109. Morphometry of perikarya or of TH-ir structures was performed on EM micrographs of typical neurons and of randomly selected TH-ir structures in all non- and TH-reacted sections. A comparison of data derived from differently fixed or immunoreacted sections (DAB without intensification, or with Ni- or SGI–intensification) did not reveal any noticeable differences in the morphometrical analyses. The procedure for the assessment of the number, kind, and associations of TH-ir structures is described below.

Controls

The specificity of the antisera was confirmed by immunoblot analysis by the supplier, and omission of the primary antibody or replacement with normal sera in the present experiments resulted in a lack of specific staining.

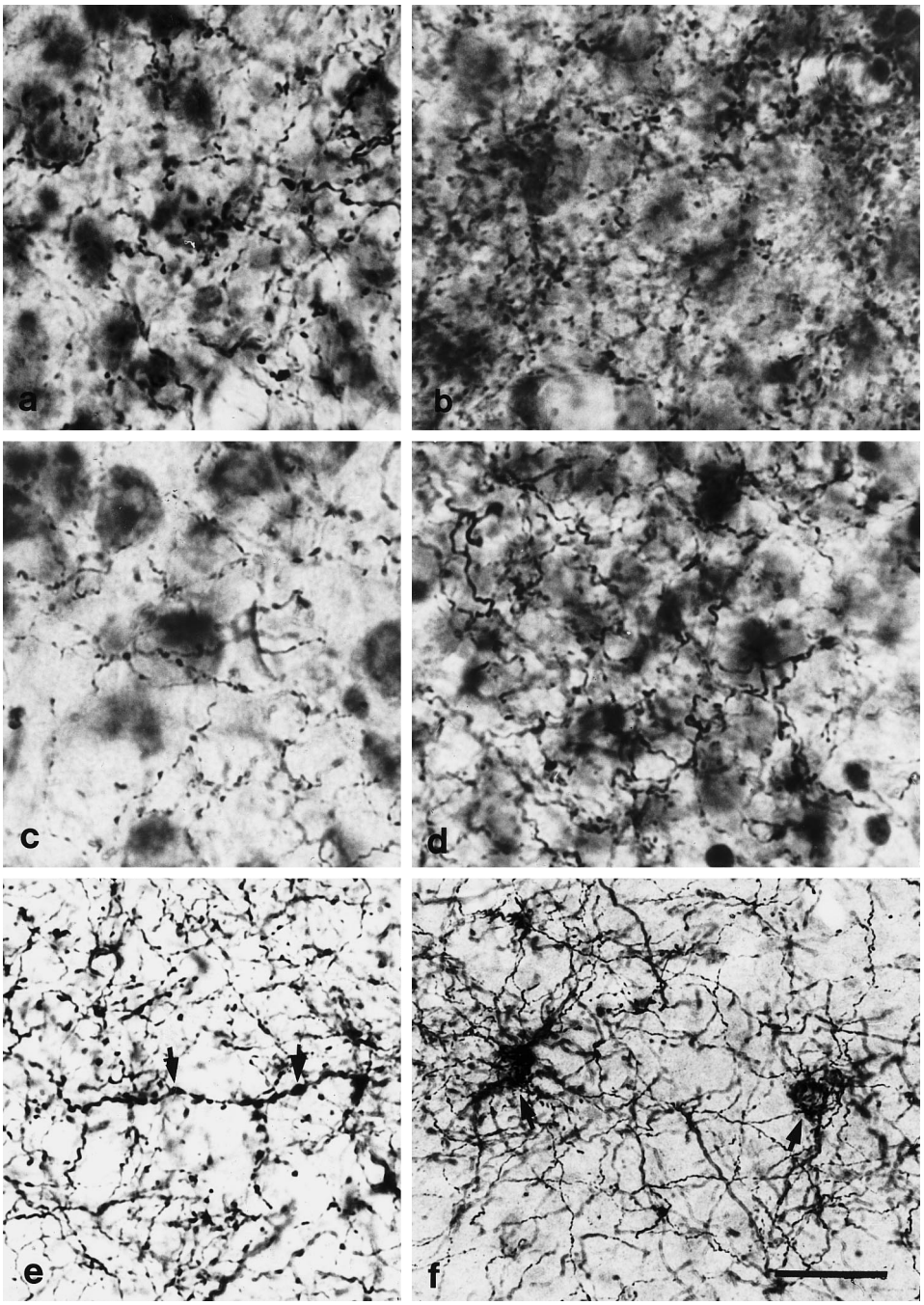

Fig. 2. TH-immunoreacted sections counterstained with cresyl violet (**a**–**d**) and not counterstained (**e**, **f**). Type A TH-ir axons in the CeM (**a**), BLP (**c**) and Ip (**d**) and type C axons in the CeLcn (**b**). **e** A type B axon in the CeM (*arrows*); **f** basket-like TH-ir fibre plexus around neurons in the BM (*arrows*). *Bar:* 20 μm

Results

Light microscopy

Cytoarchitectonic subdivisons. In the immunoreacted sections cytoarchitectonic subdivisions were defined by comparison with adjacent sections stained with cresyl violet. The nomenclature of amygdaloid nuclei used here is according to Alheid et al. (1995; Fig. 1) and that of surrounding brain regions is according to the rat brain stereotaxic atlas of Paxinos and Watson (1986).

Distribution and LM morphology of TH-ir structures. The LM findings concerning TH-ir fibres in the rat amygdala will be described here only briefly, since they have been analysed in previous studies (Fallon and Ciofi 1992; Asan 1993; Freedman and Cassell 1994). The most dense TH-ir fibre plexus were found in the paracapsular intercalated cell groups (Ips) dorsal and lateral to the lateral (L) and basolateral (BL) nuclei (Fig. 1) and in the lateral part of the anterior main intercalated cell group (Im; Fig. 1a), followed by the medial, intermediate, and lateral central parts of the CN (CeM, CeI and

Table 1. Summary of innervation characteristics of TH-ir axons in different rat amygdaloid nuclei

(Sub) Nucleus	LM axon types	EM bouton types	CPs/SPs on	Synapse types
CeM	A>>B	Narrow varicosities >> large terminals	Dendrites >>spines>> selected somata (C1)	Symmetric>>asymmetric
CeLcn	C	Small terminals	Dendrites>spines>> selected somata (C3, C4)	Symmetric>>>asymmetric
BC	A>>>B (B only in BM)	Narrow varicosities>>> large terminals (only in BM)	Dendrites>>spines>> selected somata (SPs on B1, CPs on B2, B3)	Symmetric>>>asymmetric
Ip	A	Narrow varicosities	Dendrites>spines> many somata (I1)	Symmetric

> Indicates "more frequently observed than"

CeLcn, respectively, Fig. 1a, b) and the posterior BL (BLP; Fig. 1c). Less dense plexus were observed in the anterior and ventral BL (BLA, BLV) and in the basomedial amygdaloid nucleus (BM; Fig. 1c). The lateral amygdaloid nucleus (L) and medial amygdaloid nucleus (M) possessed scarce plexus, the other nuclei, moderately dense plexus.

TH-ir terminal plexus consisted of thin, smooth axons with narrow varicosities and little branching (type A; Fig. 2a, c, d, f; Table 1). In the BM and the ventral-most tip of the BL a number of neurons was envelopped by a dense "basket-like" array of smooth fibres which extended onto proximal dendrites (Fig. 2f). Occasionally, TH-ir axons with thin intervaricose segments and large, irregularly spaced boutons were observed in CeM, CeI, BM and some other nuclei (type B; Fig. 2e; Table 1). Most TH-ir axons of the CeLcn were thin and intensely branching with a multitude of small boutons (type C; Fig. 2b; Table 1).

DBH- and PNMT-ir structures in parallel sections. DBH-immunoreacted sections exhibited dense innervation of the CeM, CeI and BL, moderately dense DBH-ir fibre plexus in the L and M, an intermediate density of fibres in the other amygdaloid nuclei and very few fibres in the CeLcn and the Is. The number of DBH-ir fibres in the L and M was as high or higher than that of TH-ir ones in parallel sections. PNMT-ir fibres were only observed in the CeM with single fibres in a few other nuclei (Asan 1993).

Most amygdaloid DBH-ir axons were smooth and somewhat wider than type A TH-ir axons, with narrow, regularly spaced varicosities. In the CeM and occasionally in the BM, DBH- and PNMT-ir axons with irregularly spaced, large varicosities and thin intervaricose segments were observed.

In area 2 of the parietal cortex, DBH labelling resulted in abundant staining of typical smooth axons in superficial layers. In contrast there were very few fibres stained in layers II–V in all studied parallel TH-immunoreacted sections, even though the TH-ir fibre staining in the adjacent caudate putamen (CPu) and amygdalae was intense (Fig. 1d–g).

Electron microscopy

Observations on the ultrastructure of neurons in CeM, CeLcn, BL, BLV, BM (basal complex; BC) and in Ips (Table 2). The preparations analysed included different subdivisions of the nuclei (e.g. the antero- and posteroventral CeM or the BL, BM and BLV). No obvious differences in neuronal morphology were discernable between the subdivisions. Since a precise delineation of the Ips in non-immunoreacted sections was not possible, analyses of the Ips' neuronal morphology was carried out exclusively on TH-immunoreacted material.

1. Central nucleus. Most CeM neurons possessed round to oval perikarya (type C1; largest diameter 13–16 μm). The nuclear envelope had indentations of varying number and size. C1 neurons had a relatively broad rim of perikaryal cytoplasm with a well-developed Golgi system. Although C1 neurons constituted a continuous morphological spectrum, this group was further divided in two subgroups. Type C1a neurons possessed more or less abundant stacks of cisterna of rough endoplasmic reticulum (rER), somatic spines were not encountered and between three and five axosomatic synapses were found (Fig. 3a). Type C1b neurons had scattered cisternae of rER, occasionally possessed small somatic spines, and the number of axosomatic synapses was somewhat higher (see below). Less frequent than C1 neurons were smaller (largest diameter 8–10 μm), round neurons with shallow nuclear indentations and a narrow rim of cytoplasm with few organelles and single somatic spines (type C2; Fig. 3b).

In the CeLcn, two types of neurons were about equally frequently observed. Round neurons (Type C3; largest diameter 10–14 μm; Fig. 4a) possessed a round nucleus

Table 2. Some ultrastructural characteristics of perikarya of neuron types encountered in different rat amygdaloid nuclei

Neuron type	Occurrence		Perikaryal size (μm)	Shape	Nuclear shape	Organelles		Additional characteristics
a. Central nucleus:								
C1a, b	CeM CeLcn	+++ +	13–16	Round to oval	Irregular, deep indentations	Golgi C1a: rER C1b: rER	++ +++ +	C1a: Somatic spines not observed C1b: Few, small somatic spines symmetric axosomatic synapses
C2	CeM	+++	8–10	Round	Round, shallow indentations	Golgi rER	(+) (+)	Few somatic spines; symmetric axosomatic synapses
C3	CeLcn	+++	10–14	Round	Round, no indentations	Golgi rER	+ +	Somatic spines: C3>C4; extensive somatosomatic and somatodendritic appositions; symmetric axosomatic synapses
C4	CeLcn	+++	12–19	Oval	Oval, no indentations	Golgi rER	++ ++	
b. Basal complex:								
B1	BC	+++	14–18	Round to oval to pyramidal	Round to oval, some indentations	Golgi rER many others	+++ ++	Small somatic spines; many symmetric axosomatic synapses
B2	BC	+	11–13	Similar to B1	Irregular, deep indentations	Golgi rER	++ +++	Somatic spines not observed; symmetric axosomatic synapses
B3	BC	+	8–11	Oval to round	Similar to B2	Golgi rER	+ +	Large somatic spines; symmetric and asymmetric axosomatic synapses
c. Paracapsular intercalated nuclei:								
I1	Ip	+++	8–11	Round to oval	One or two small indentations	Golgi rER	++ ++	Small somatic spines; extensive somatosomatic appositions; symmetric axosomatic synapses
I2	Ip	(+)	Similar to B2 (see above)					

+++ Abundant, ++ several, + scattered, (+) very few

without indentations, a comparatively narrow rim of cytoplasm with a number of small Golgi stacks and mitochondria as well as other organelles, but with little rER. Somatic spines were rare, but dendritic spines were encountered on proximal dendrites. Extensive symmetric axosomatic synapses were observed. Some of the contacting terminals contained a variety of different vesicles (Fig. 4b). Type C4 neurons (Fig. 4a) possessed an oval nucleus without indentations and an oval soma (largest diameter 12–19 μm) with a cytoplasmic rim which was broader than that of type C3 neurons. They had more, albeit irregularly scattered, rER cisternae and larger Golgi stacks sometimes extending into proximal dendrites. Somatic spines were more frequently observed and axosomatic synapses less frequently observed than in type C3 neurons (Fig. 4a). Occasionally, neurons similar to types C1 and C2 (see above) were found in the CeLcn (about every tenth neuron).

A number of unusual organelles were observed in central nucleus neurons, such as cilia, lamellar bodies and subsurface lamellae which were continuous with rER cisternae (Fig. 4a, c). In the CeLcn close apposition of the plasma membranes of two somata (Fig. 4a, d) or of a soma and a proximal dendrite was observed frequently. Within these apposition zones the membranes appeared fused or thickened. Membranous vesicles and saccules were found in the vicinity of the apposed membranes, and the nuclei were located excentrically near the apposition zones (Fig. 4d).

2. Basal complex. The most frequent neuron type (B1; largest diameter 14–18 μm) possessed a round to oval, light nucleus with more or less deep nuclear indentations, abundant cytoplasm with well-developed Golgi apparatus and scattered rER cisternae. The somata had a pyramidal, round or oval shape (Fig. 5a, b). Symmetric axosomatic synapses (more than five in one sectional plane) and small somatic spines were observed (Fig. 5a). Types B2 and B3 were less frequent (about every seventh neuron). B2 had a smaller soma than B1 (largest diameter was 11–13 μm), was similarly shaped and possessed a darker nucleus with a multitude of deep invaginations. It had a broad cytoplasmic rim with many organelles, especially with abundant stacks of rER cister-

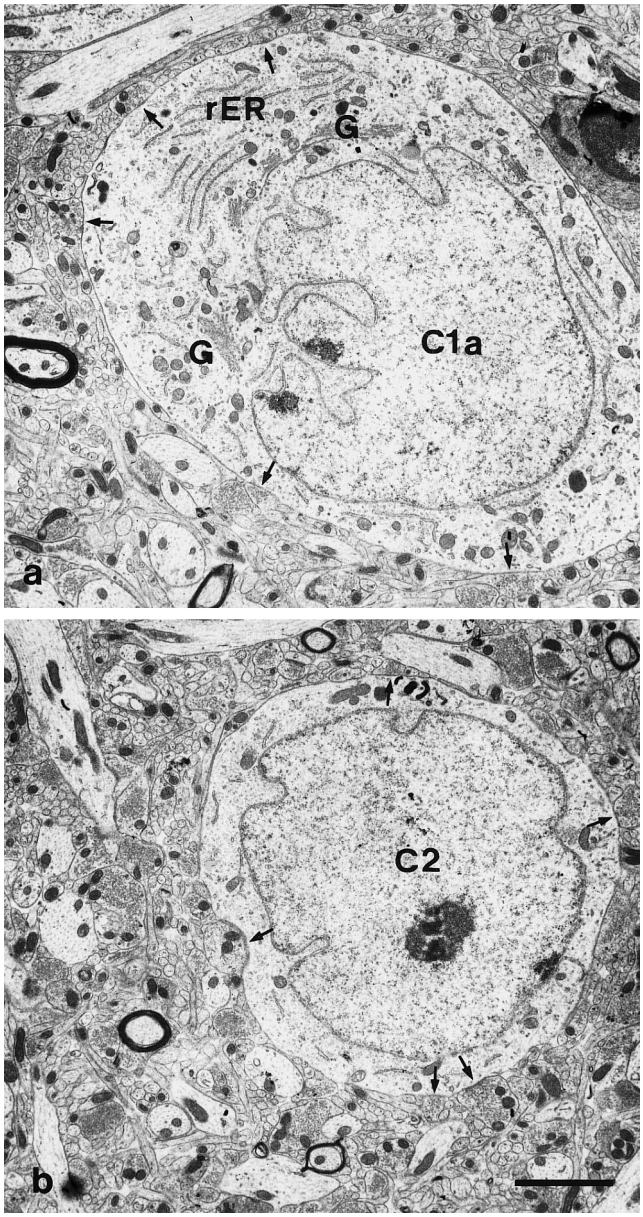

Fig. 3. Typical *C1a* (**a**) and *C2* (**b**) neurons in the CeM. *Arrows* point to axosomatic synapses. *G*, Golgi stacks; *rER*, rough endoplasmic reticulum. *Bar:* 2 μm

nae (Fig. 5b, c). Symmetric axosomatic synapses were less frequent than on B1 and somatic spines were not observed. Type B3 possessed the smallest somata (largest diameter was 8–11 μm), which were either oval or round, and had a deeply indented nucleus and a narrow cytoplasmic rim (Fig. 5d). Asymmetric axosomatic synapses were observed. Some B3 neurons possessed large somatic spines on which asymmetric synapses were formed (Fig. 5e).

3. Paracapsular intercalated cell groups. The vast majority of neurons were small (largest diameter was 8–11 μm) with round or oval nuclei which had one or two nuclear indentations (type I1; Fig. 11a). The cytoplasmic rim was broad and contained, among other organelles, a few small Golgi stacks and scattered rER cisternae. Lamellar bodies were frequently encountered. A number of axosomatic contacts forming symmetric synapses and somatic spines were observed. The neurons were clustered closely together, and many somata had extensive appositions with one or more other somata (Fig. 11a). In several cases lamellar bodies were situated directly adjacent to apposed membranes (Fig. 11b), and structures resembling specialized contacts were encountered (Fig. 11c). Very rarely a larger neuron was observed between the small ones (type I2), with a deeply indented nucleus and abundant cytoplasm. This type was similar to B2 neurons of the BC (see above).

Ultrastructural features of TH-ir structures in the CeM, CeLcn, BC and Ips (Table 1). Sections for EM analyses of the CN and BC were taken from different rostrocaudal levels containing different subdivisions; Ip sections were taken from dorsal or lateral Ips (cf. Fig. 1a, c).

1. General ultrastructural characteristics of TH-ir elements. TH immunoreactivity was found exclusively in unmyelinated axons, with immunoreaction product homogeneously distributed in the axonal cytoplasm and attached to membranes such as those of mitochondria. Small clear round vesicles could be identified in many TH-ir axons (e.g. Fig. 6e). Occasionally, the presynaptic region with its dense clusters of vesicles was less immunoreactive than the rest of the terminal (Fig. 6e). Boutons contained zero to three mitochondria. Large dense-cored vesicles (LGVs) were only rarely identified, but were always found in unusually large and lightly labelled terminals (>1 μm). The latter were rare on the whole, but more frequent in the CeM than in the CeLcn and BC and were absent from the Ips. In the BC they were restricted to the BM (not shown; Asan 1993).

In serial sections, the majority of TH-ir elements contacting unlabelled neuronal elements were found to form synapses. Several criteria were applied for the identification of synaptic contacts. Presynaptic vesicle accumulations and pronounced densities of the postsynaptic membranes were considered proof of synaptic contacts. Synapses were classified as asymmetric if the synaptic clefts were widened and the postsynaptic densities were especially prominent. They were considered symmetric if the cleft was narrower and the postsynaptic membranes less dense than in asymmetric synapses in the vicinity (Peters et al. 1991). Due to the fact that presynaptic vesicle accumulations were mostly obscured by immunoreaction product, and since postsynaptic membranes of symmetric synapses by definition are rather inconspicuous, it was sometimes difficult to discern symmetric synapses. Nevertheless, clearly symmetric synapses were more frequent than asymmetric ones. Some of the rare larger terminals (see above) were observed to form asymmetric synapses on dendrites or spines (not shown; Asan 1993). Identification of spines was carried out either in serial sections or according to the criteria of Peters et al. (1991).

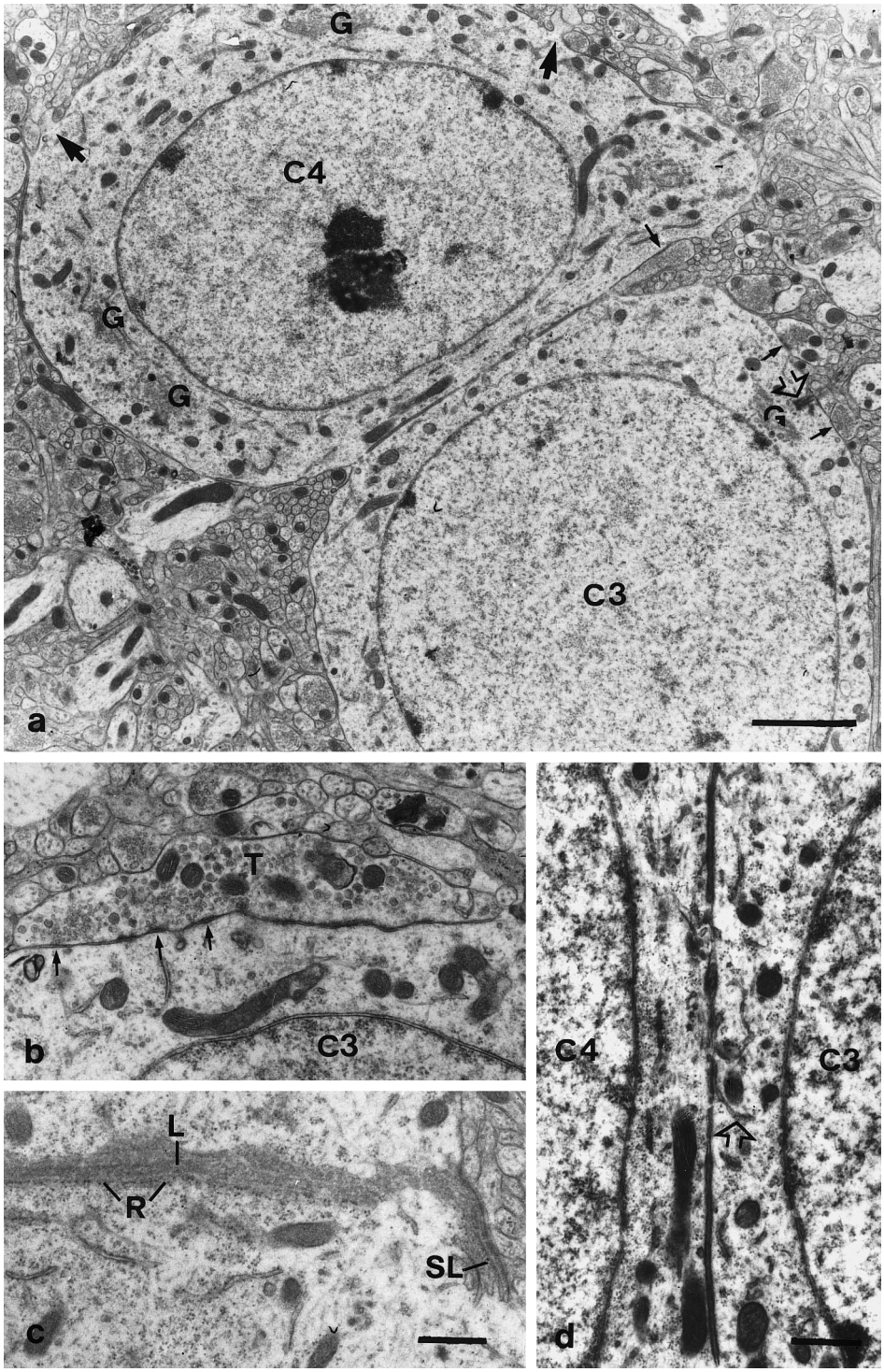

Fig. 4. a Typical *C3* and *C4* neurons in the CeLcn. *Large arrows* point to somatic spines, *small arrows*, to axosomatic synapses and the *open arrow*, to the origin of a cilium. *G*, Golgi stacks. *Bar:* 2 μm. **b** Large terminal (*T*), containing different forms of vesicles and forming symmetric synaptic contacts (*arrows*) with a *C3* neuron. **c** Subsurface lamellae (*SL*) in continuity with a large lamellar body (*L*) whose lowest lamella is bearing ribosomes (*R*). *Bar* in **c**: 0.5 μm (same magnification in **b**). **d** Enlargement of the apposition zone of the two neurons in **a**. Membrane thickenings, fusion zones, and membranous structures (*open arrow*) are visible. *Bar:* 0.5 μm

2. Central nucleus. In the CeM thin TH-ir axons (diameter <0.2 μm; Fig. 6a) with narrow varicosities (<0.9 μm; Fig. 6b) and occasional swellings at branching sites (Fig. 6c) were observed which formed en passant synapses with small- to medium-sized dendrites (Fig. 6b, c). Contacts or synapses on dendritic spines were less frequent.

In the CeLcn, longitudinal sections of intervaricose segments were rare while transverse sections were frequent (diameter <0.2 μm; Fig. 6d). Groups of small TH-ir terminals were found (diameter <0.9 μm) which formed synapses on dendrites (Fig. 6d) and dendritic spines, the latter being contacted on their necks (Fig. 6e) or heads (Fig. 6f). A contact on a somatic spine was observed once (not shown).

Both in the CeM and CeLcn, the majority of synapses formed by TH-ir axons were symmetric (Fig. 6b, d–f); however, asymmetric ones were also observed (Fig. 6c).

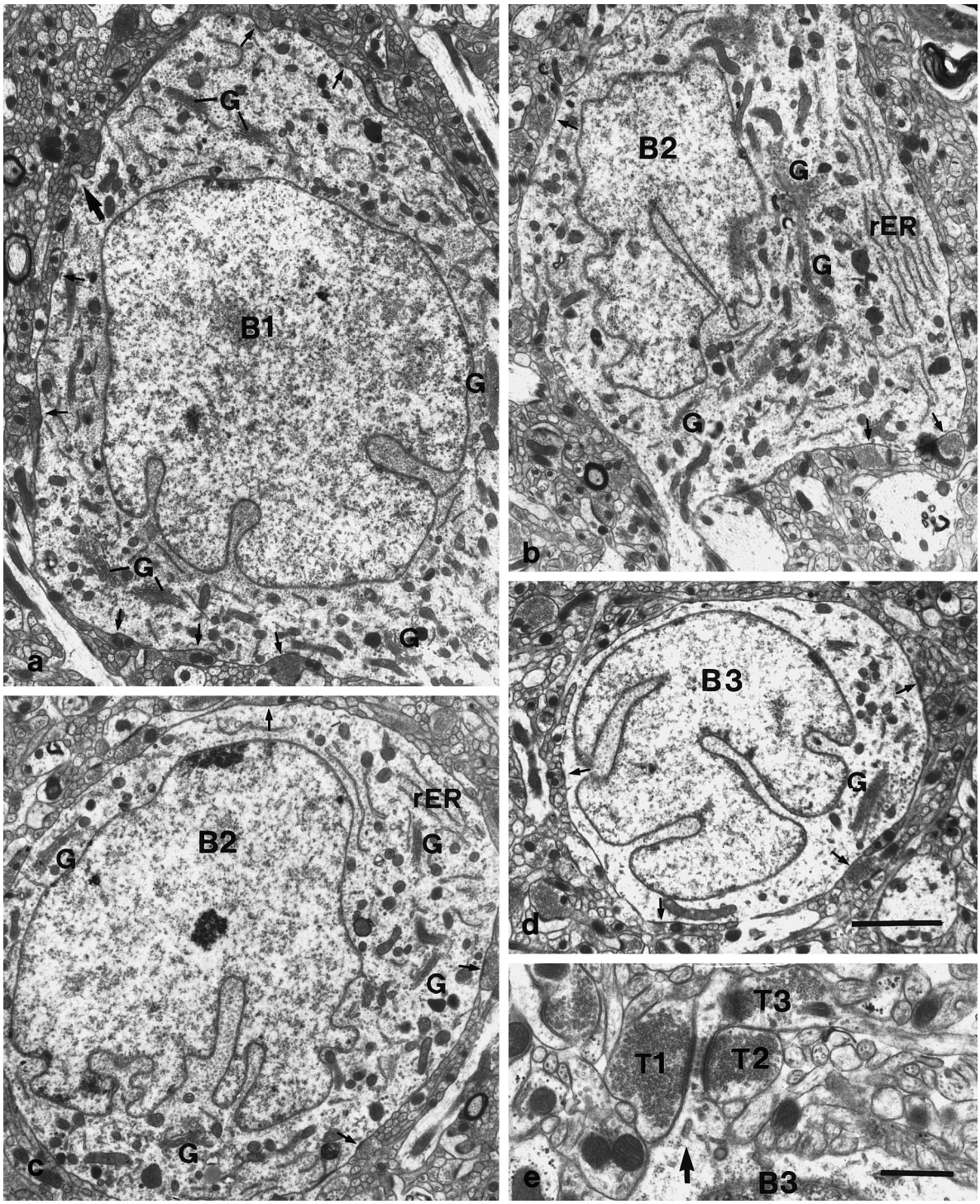

Fig. 5. **a** *B1* neuron of the BC with a pyramid-shaped perikaryon. **b**, **c** *B2* neurons with a pyramidal (**b**) and round (**c**) perikaryon. **d** *B3* neuron. **e** Somatic spine of a *B3* neuron receiving asymmetric synapses from three terminals (*T1–3*). **a**–**e** *Large arrows* point to somatic spines; **a**–**d** *small arrows* point to axosomatic synapses; *G*, Golgi stacks; *rER*, rough endoplasmic reticulum. Bars: 2 μm in **d** (same magnification in **a**–**c**); 1 μm in **e**

Neuronal elements contacted by TH-ir axons were usually additionally contacted by other, unlabelled terminals (Fig. 6b, e, f). In the CeLcn, the combination of a symmetric synapse of a TH-ir terminal on a spine in the vicinity of an asymmetric synapse formed by an unlabelled terminal on the same spine was observed a number of times (Fig. 6f). Very often, TH-ir axons were found in direct apposition to unlabelled terminals (Fig. 6b, d). Especially in the CeLcn these appositions appeared to be more than casual membrane encounters, even though axoaxonic synapses could not be clearly identified (Fig. 6g).

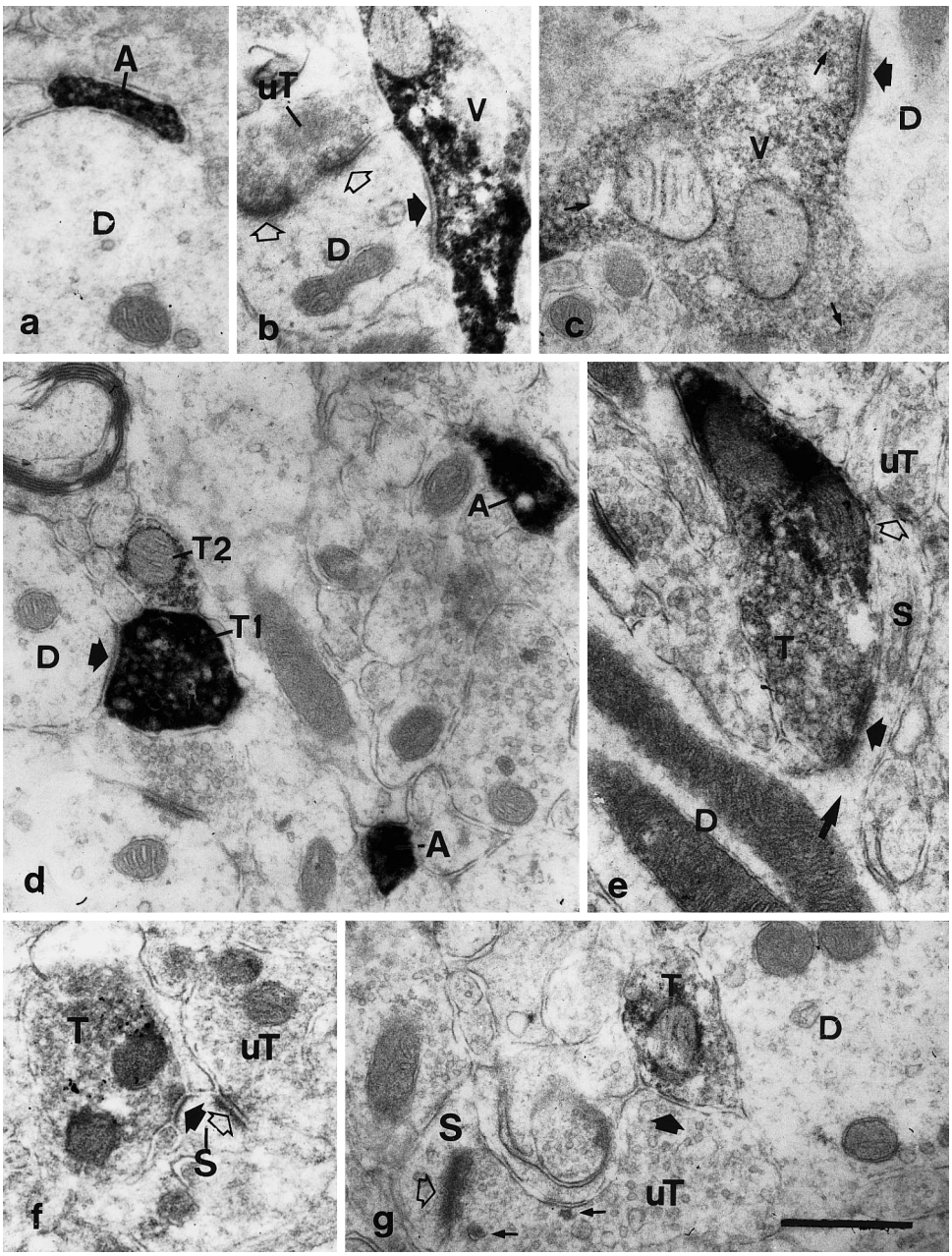

Fig. 6. a–c TH-ir intervaricose axon (**a**), varicosity (*V*, **b**) and axonal branching point (*V*, **c**) in the CeM. The varicosity in (**b**) forms a symmetric synapse (*filled arrow*) with a small dendrite (*D*), which also receives asymmetric contacts (*open arrows*) from an unlabelled terminal (*uT*). The branching point (**c**) forms an asymmetric synapse (*large arrow*) with a small dendrite (*D*). *Small arrows* indicate the direction of the axon and daughter branches. **d**–**g** TH-ir axons and terminals in the CeLcn. **d** A TH-ir terminal (*T1*) forms a symmetric synapse (*arrow*) with a small dendrite (*D*). A second TH-ir terminal (*T2*) is more lightly labelled. *A*, Intervaricose axons. **e** A TH-ir terminal (*T*), in which the presynaptic area with dense accumulation of vesicles is more lightly labelled than the rest of the axoplasm, possesses a symmetric synapse (*small arrow*) with a dendritic spine (*S*; *large arrow*), which is also contacted by an unlabelled terminial (*uT*, *open arrow*). **f** A small spine (*S*) possesses a symmetric synapse (*filled arrow*) with a TH-ir terminal (*T*) and an asymmetric synapse (*open arrow*) with an unlabelled terminal (*uT*). **g** A weakly TH-ir terminal (*T*) is apposed to an unlabelled terminal (*uT*) which forms an asymmetric synapse (*open arrow*) with a small spine (*S*). *Small arrows* Large dense-cored vesicles. **a**–**e**, **g** Ni-DAB intensification; **f** SGI–DAB intensification. *Bar:* 0.5 μm

In both subnuclei contacts with neuronal somata were found. However, counting of neuronal perikarya in defined areas of ultrathin sections (see below) revealed that only about one in 20 (CeM) or one in 15 (CeLcn) neuronal somata were contacted per sectional plane. In the CeM, contacted neurons were of type C1b (see above; Table 2; Fig. 7), and TH-ir axons with typical narrow varicosities were observed to be running along the soma membrane for long distances and forming symmetric synapses in their course (Fig. 7a–c). In the CeLcn, C3- and C4-type neurons were contacted by small terminals, forming symmetric synapses on various points of the entire circumference of the neuron (Fig. 8).

3. Basal complex. The ultrastructural morphology of TH-ir axons in the BC was similar to that found in the CeM. En passant-type contacts with unlabelled structures were even more common (Fig. 9a–e). In the BM a larger TH-ir varicosity was observed "capping" a medium-sized dendrite, which possessed another contact and was observed in serial sections to be apposed to a narrow axon over a long distance (Fig. 9a, b). Contacts on dendrites (Fig. 9d) were more common than on spines (Fig. 9c). A few asymmetric contacts were observed (Fig. 9e), and postsynaptic elements possessed asymmetric or symmetric synapses from unlabelled terminals in close vicinity (Fig. 9c). En passant contacts were observed on neuronal somata, usually of type B1, and symmetric synapses could be identified (Fig. 10). Appositions without clear synaptic specializations were found on a few type B2 (Fig. 10c) and B3 neurons (not shown). As in the central nucleus, only few somata were contact-

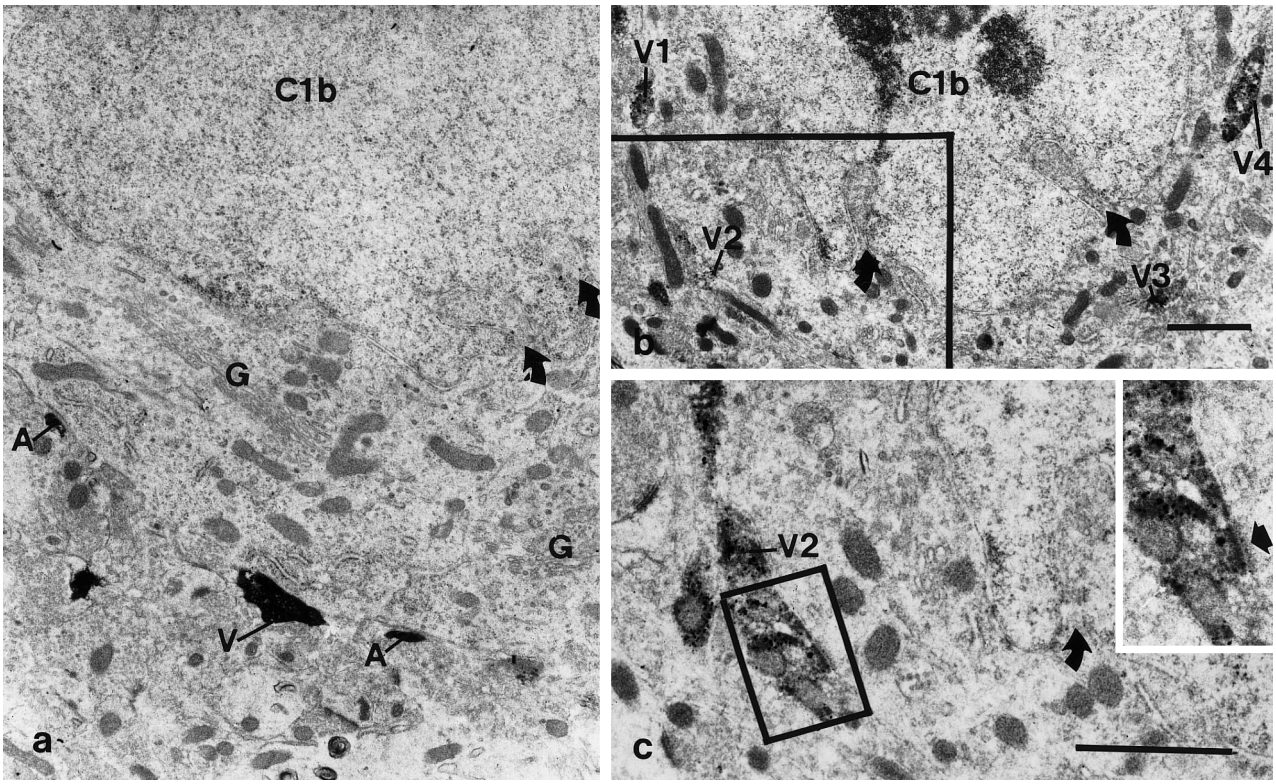

Fig. 7a–c. Contacts of TH-ir varicosities on *C1b* neurons of the CeM. *Curved arrows* point to typical indentations of the nuclear envelope. **a** A varicosity (*V*) contacts a *C1b* neuron; two intervaricose axons (*A*) are close to the plasmalemma. *G,* Golgi. **b** Several varicosities (*V1–4*) contact a *C1b* neuron. **c** Enlargement of the *boxed area* in **b** in a serial section. The continuation of *V2* is seen to contact the C1b neuron. The *inset* shows an enlargement of the *boxed area* with a symmetric synaptic contact (*arrow*). **a** NiDAB intensification; **b**, **c** SGI–DAB intensification. *Bars:* 1 μm in **b** (same magnification in **a)**; 1 μm in **c**

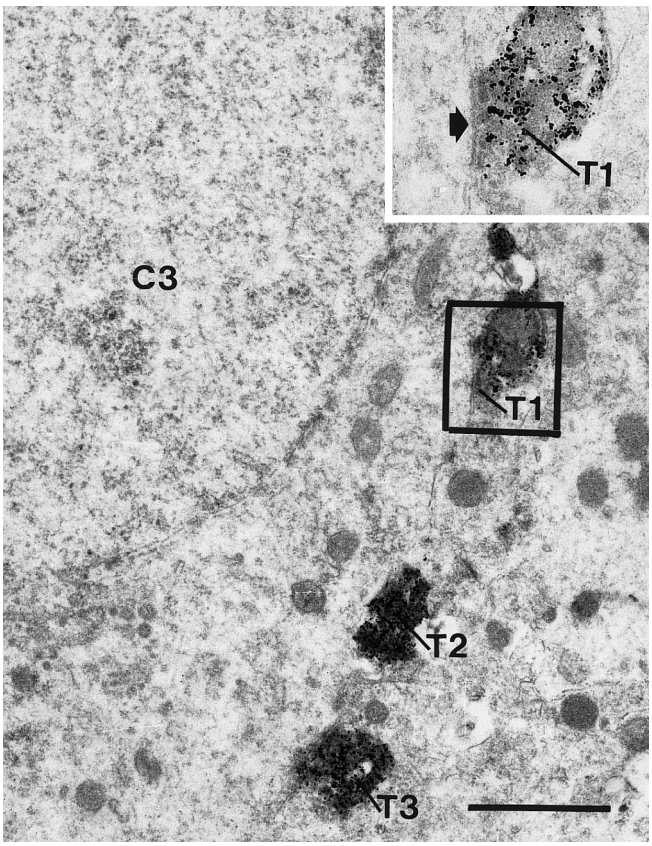

ed, but those that were almost always possessed more than one contact in single sectional planes (Fig.a, c).

4. Paracapsular intercalated cell groups. A number of TH-ir small terminals and narrow varicosities were observed (Fig. 11a, d–g). As in the other nuclei, many appositions were found on dendrites and spines, and again the postsynaptic elements received synapses from unlabelled terminals in close vicinity (Fig. 11g). In contrast to the situation in the central and basal nuclei, the majority of I1-type neurons (36 of 63 somata observed) were contacted by TH-ir terminals, many of them by more than one terminal or by a narrow axon or varicosity apposed to the somatic plasmalemma (Fig. 11a, d). Also, some of the contacted dendrites were rather large, and some of the contacted spines were somatic spines (Fig. 11e). Synapses were formed with all types of elements contacted and possessed exclusively symmetric specializations (Fig. 11d, f, g).

Fig. 8. Three TH-ir terminals (*T1–3*) contact a *C3* neuron in the CeLcn. The *inset* shows an enlargement of the boxed area in a serial section with a symmetric synaptic contact (*arrow*). This neuron is additionally contacted by three other TH-ir terminals (not shown). SGI–DAB intensification. Bar: 1 μm

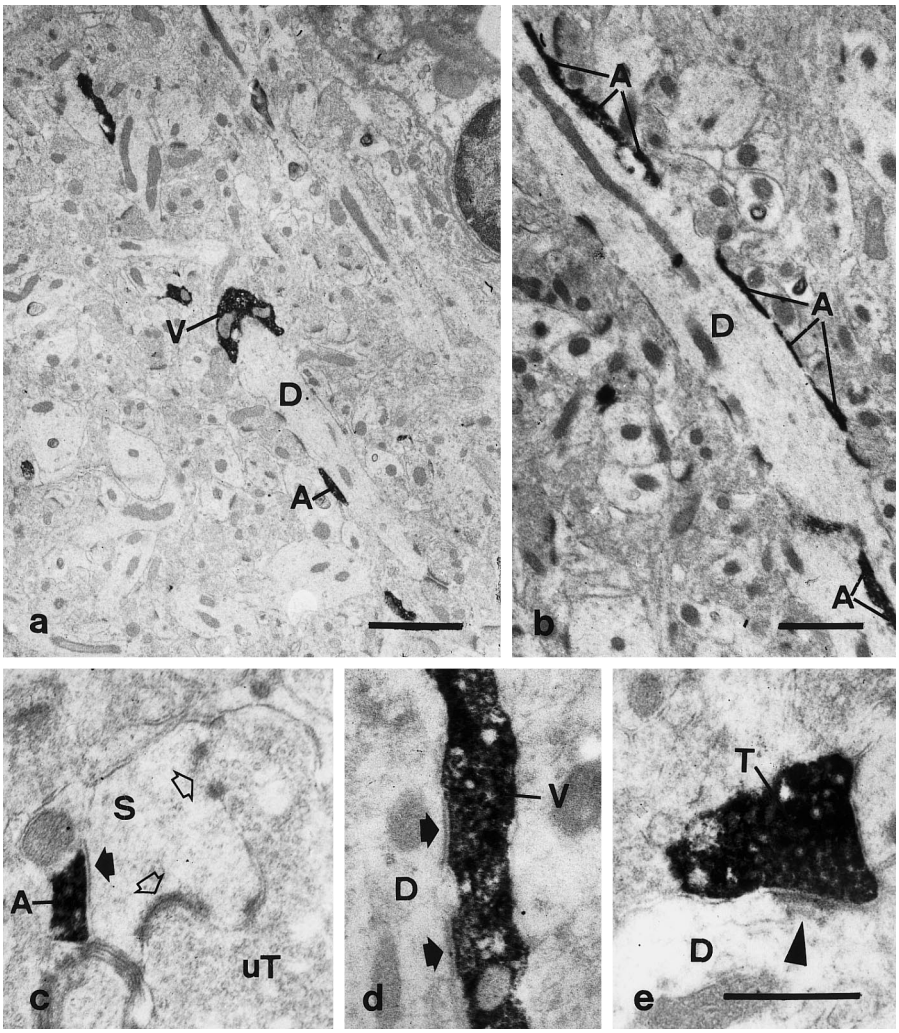

Fig. 9a–e. TH-ir axons (*A*) and varicosities (*V*) in the BC. **a** A small dendrite (*D*) is capped by a large varicosity (*V*) and contacted by a narrow axon (*A*). **b** In a serial section, TH-ir axons (*A*) are apposed to the dendrite shown in **a** over a long distance and at different points. **c** A narrow TH-ir axon forms a symmetric synapse (*filled arrow*) with a spine (*S*) which receives asymmetric synapses (*open arrows*) from a large unlabelled terminal (*uT*). **d** A narrow varicosity (*V*) forms two en passant symmetric synapses (*arrows*) with a small dendrite (*D*). **e** A somewhat larger terminal forms an asymmetric synapse (*arrowhead*) with a small dendrite (*D*). NiDAB intensification. *Bars:* 2 μm in **a**; 1 μm in **b**; 0.5 μm in **e** (same magnification in **c** and **d**)

Quantitative analyses

For the CeM, CeLcn and BC, three squares of the 200 mesh thin-bar nickel grids (approx. 40000 μm^2) were analysed per ultrathin section taken from different interaural levels (IALs) of three brains. Since the Ips were too small to fill even one square, the entire Ip area as defined by the presence of I1-type neurons was analysed in ultrathin sections from three brains (one dorsal Ip and two lateral Ips). To check for intraindividual variability, three different ultrathin sections were analysed for the CeLcn of brain A1: two from the upper and lower surfaces of one vibratome section at an IAL of ca. 6.7 according to Paxinos and Watson (1986), the other from a second Vibratome section of IAL 6.4. Also, two ultrathin sections from the BC of brain A1 were analysed (Fig. 12). Smaller scale analyses carried out for all nuclei in sections from the other studied brains were in the range documented for brains A1–A3 below.

All TH-ir profiles in the defined areas within the nuclei were counted. The absolute number of TH-ir profiles counted per section analysed varied (154–325 for CeM, 205–516 for CeLcn, 101–269 for BC and 40–133 for the Ips). Comparison of counts from different nuclei that were taken from the same Vibratome sections showed that the numbers of profiles were slightly to moderately higher in the CeLcn than in the CeM and considerably lower in the BC (CeLcn/CeM, 322/318 for A1; CeLcn/CeM/BC, 205/154/101 for A2; CeLcn/CeM/BC, 359/325/211 for A3).

Since the qualitative analysis had shown that many synapses were established by narrow axons en passant, all profiles that were closely apposed to neuronal elements were classified as “contacting profiles” (CP). Those CPs that formed synapses were rated as “synaptic profiles” (SP). CPs and SPs were further classified according to the target of the apposition or synapse (somata, dendrites or spines). Direct appositions with unlabelled axons were not separately registered. In the intraindividual comparison of the three sections analysed for the A1 CeLcn and of the two sections analysed for the A3 BC, the percentage values calculated for the differently targeted CPs/SPs among all CPs/SPs lay closely together (Fig. 12), with a variation range of less than 10% for all and less than 5% for most values. Larger variations were found for some relative values in the in-

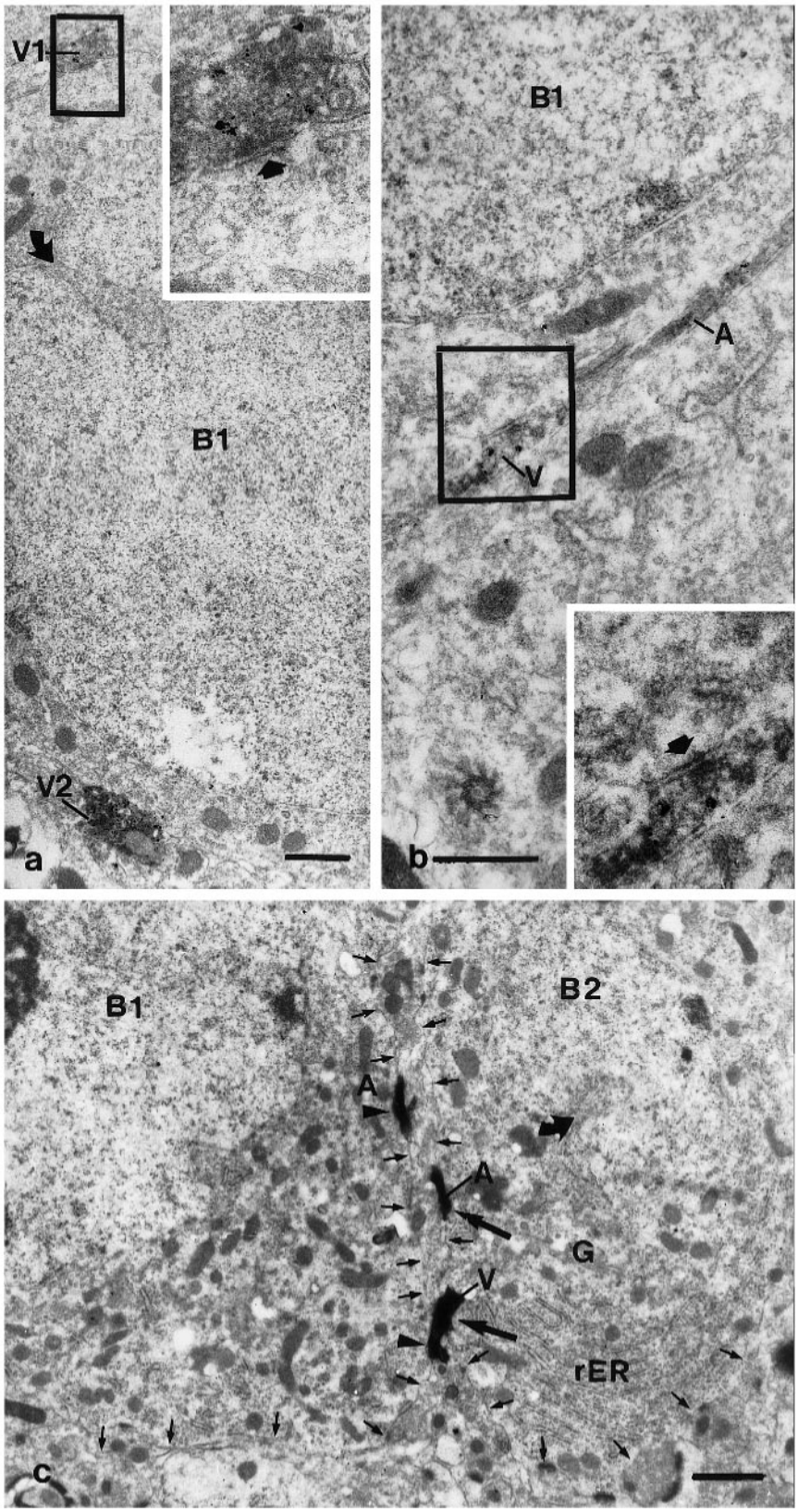

Fig. 10a–c. Contacts of TH-ir axons and varicosities with neurons in the basal complex. **a** Two TH-ir varicosities (*V1* and *V2*) contact a *B1* neuron. The *curved arrow* points to a typical shallow indentation of the nuclear envelope. *Boxed area* is enlarged in the *inset*, which shows a symmetrical synaptic contact (*arrow*). **b** A narrow TH-ir axon (*A*) runs wedged between two closely apposed somata, one of which belongs to a *B1* neuron. A narrow varicosity (*V*, *boxed area*) forms a symmetric synaptic contact with the *B1* neuron shown in the *inset* (*arrow*). **c** TH-ir axon (*A*) with a narrow varicosity (*V*) runs between a *B1* and a *B2* neuron. Although only part of the nucleus of the *B2* neuron is sectioned, one of the typical deep indentations of the nuclear envelope is visible (*curved arrow*). Also seen are Golgi stacks (*G*) and the typical abundant rough endoplasmic reticulum (*rER*). The cell borders of the two neurons are indicated by *small arrows*. *V* is in contact with both the *B1* (*arrowheads*) and the *B2* neuron (*large arrow*), while one *A* contacts the *B2* neuron (*large arrow*), the other *A* contacts the *B1* neuron (*arrowhead*). **a**, **b** SGI–DAB intensification; **c** Ni-DAB intensification. *Bars:* 1 μm

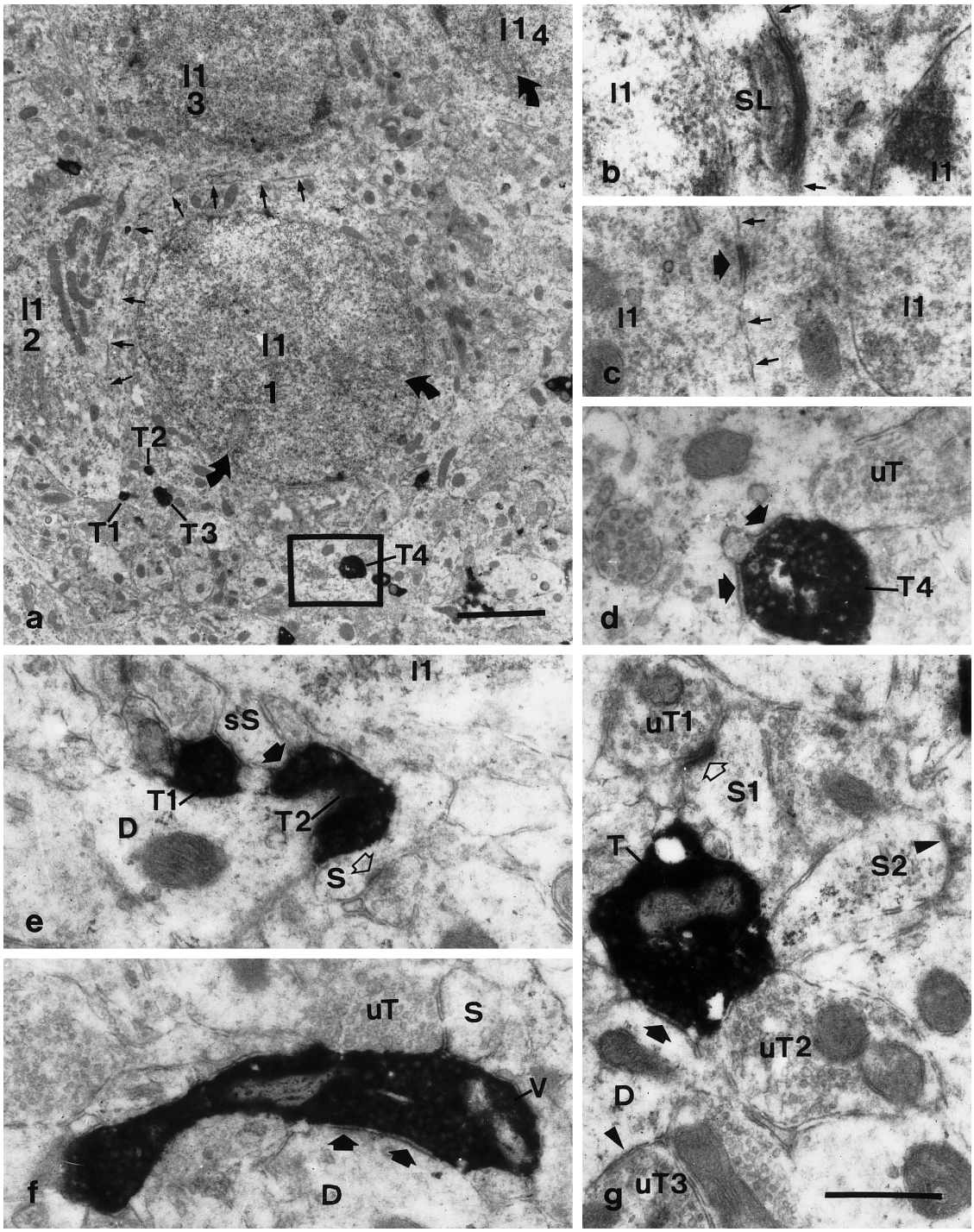

Fig. 11a–g. Typical I1 neurons and TH-ir elements in the paracapsular intercalated cell groups. **a** Four *I1* neurons are visible. *Curved arrows* point to typical indentations of the nuclear envelope, *small arrows*, to the plasma membrane of neuron *I1/1*, which is closely apposed to neurons *I1/2* and *I1/3*. *I1/2* is contacted by a small TH-ir terminal (*T1*), *I1/1* is contacted by three TH-ir terminals (*T2–4*). **b**, **c** Characteristics of neuronal apposition zones. *Small arrows* point to apposing membranes. **b** Shows subsurface lamellae (*SL*) directly beneath the apposing membrane of one of the neurons. **c** Shows thickened membranes at the apposition zone of two other neurons (*large arrow*). **d** Is an enlargement of the *boxed area* in **a**, showing symmetric synaptic contacts of the TH-ir terminal *T4* onto neuron I1/1. *T4* is adjacent to an unlabelled terminal (*uT*) which is also in direct contact with I1/1. **e** Two TH-ir terminals (*T1* and *T2*) are apposed to a small somatic spine (*sS, filled arrow*) of an *I1* neuron. They are also apposed to a small dendrite (*D*), and *T2* is additionally apposed to a small spine (*S*) which receives an asymmetric synaptic contact (*open arrow*). **f** A TH-ir varicosity (*V*) forms a long symmetric synapse (*arrows*) with a small dendrite (*D*). *V* is also apposed to an unlabelled terminal (*uT*) and to a small spine (*S*). **g** A TH-ir terminal (*T*) forms a symmetric synapse (*filled arrow*) on a small dendrite (*D*), which is also contacted by an unlabelled terminal (*uT3*). *T* is additionally apposed to another unlabelled terminal (*uT2*) and to two spines (*S1* and *S2*). *S1* receives an asymmetric synapse (*open arrow*) from a third unlabelled terminal (*uT1*). *S2* also receives an additional synaptic contact (*arrowhead*). NiDAB intensification. *Bars:* 2 μm in **a**; 0.5 μm in **g** (same magnification in **b**–**f**)

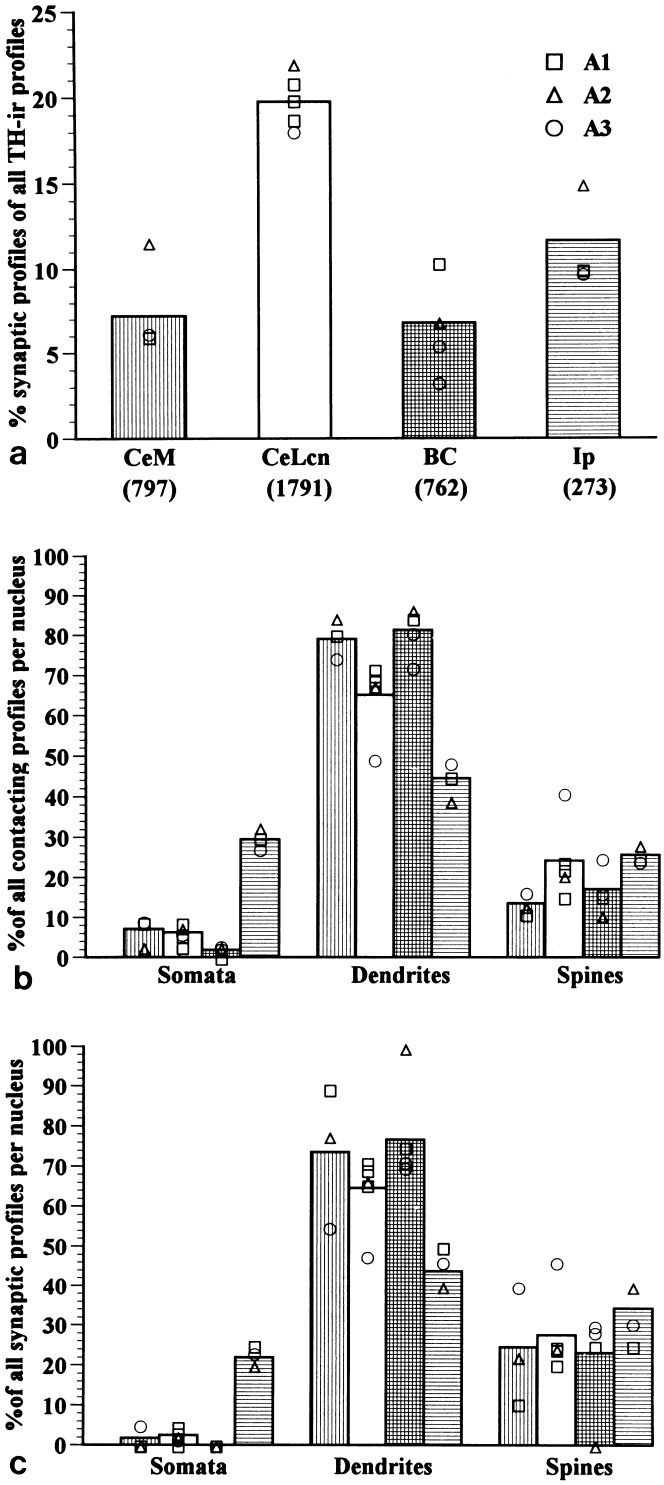

Fig. 12a–c. Results of quantitative investigations. *Columns* indicate mean values calculated for all sections; *symbols* signify values derived from individual sections from different brains (*A1*, *A2*, *A3*). For the *CeLcn*, three different sections from brain *A1*, and for the *BC*, two different sections from brain *A3* were analysed. **a** Percentages of synaptic profiles in different nuclei. *Numbers below the abscissa* indicate counted profiles in the respective nuclei. **b**, **c** Percentages of contacts and synapses among all contacting and synaptic profiles, respectively. *Column patterns* represent different nuclei as shown in **a**

terindividual comparison, usually because the analysis for one brain differed from those of the others, which again lay within a 10% range (Fig. 12).

Synaptic density. The proportion of synapses among all TH-ir profiles in single sections of different nuclei exhibited little intra- and interindividual variations (Fig. 12a). The highest synaptic density was found in the CeLcn, where 355 (19.8%) of 1791 TH-ir profiles formed identified synapses. In the CeM, the density was significantly lower – of 797 TH-ir profiles 57 (7.2%) were SPs. An intermediate density was found in the Ips, where 32 (11.7%) of 273 TH-ir profiles were SPs. The synaptic density of the BC was in the range of the CeM with 52 (6.8%) of 762 TH-ir profiles being SPs. Thirty-nine (11%) of all the synapses in the CeLcn, 8 (22%) synapses in the CeM and 2 (3.9%) synapses in the BC, were classified as asymmetric. Among these, a few were formed by the large type of TH-ir axonal boutons. No asymmetric synapses were recognized in the Ips. With respect to asymmetric synapses, the differences between individual analyses were rather large: their contribution ranged from 4.4% to 21.3% in the CeLcn, from 5.3% to 27.8% in the CeM, and from 0% to 7.1% in the BC.

Targets of contacts. The percentage of contacts and synapses on somata was about equally high in both central nucleus subdivisions and was lower in the BC (Fig. 12b, c). In the Ips, the values were more than fourfold higher than in the central nucleus, constituting about 30% (20%) of the contacted (synaptic) targets.

In all analyses of all nuclei, contacts and synapses on dendrites were more frequent than those on spines; however, relatively more contacts on spines were found to be synaptic than on dendrites (Fig. 12b, c). The relative frequency of contacts on dendrites as compared to contacts on spines was higher in the CeM and BC than in the CeLcn and Ips, indicating that in the two latter nuclei spines were more often the target of TH-ir afferent fibres than in the CeM and BC. All asymmetric synapses detected were localized on dendrites and spines, and most of them (six of eight in the CeM, 27 of 39 in the CeLcn, and one of two in the BC) were formed with spines. In the case of the CeLcn, 18 synaptic target structures (5.1%), four of them with asymmetric synapses, could not be unequivocally identified as small dendrites or spines. These are not represented in the figures but will be discussed below.

Discussion

The qualitative and quantitative analyses show that, although the TH-ir axons innervating different amygdaloid nuclei possess similar characteristics as judged by LM and EM, certain aspects of the innervation pattern differ not only between the nuclei, but also between subnuclei (summarized in Table 1).

General ultrastructural features of amygdaloid TH-ir axons and terminals

Qualitative studies. In the CeM, BC and Ips most contacts were formed by TH-ir varicosities or narrow axons en passant, while in the CeLcn small terminals prevailed. This finding agrees well with the light-microscopic morphology of type A axons in the CeM, BC and Ips and of type C axons in the CeLcn. Otherwise, the axonal morphology was similar in all nuclei. All TH-ir axons found were unmyelinated, contained round clear vesicles, and in the majority LGVs were not identifiable. They formed mainly symmetric synapses (Peters et al. 1991). Dendritic shafts and spines were the preferential targets of TH-ir afferent fibres and often received additional input from unlabelled terminals. Contacted somata usually possessed more than one TH-ir apposition in single sectional planes.

Quantitative studies. The quantitative evaluation supported the qualitative impressions. In the documentation of the results mean values calculated from all section analyses are shown together with the values for the individual analyses (Fig. 12) to enable recognition of intra- and interindividual variations within and between the different categories.

Since identification of symmetric synapses was sometimes difficult, and because most TH-ir terminals contacting neuronal elements were found to form distinct symmetric synapses in serial sections, the registration of contacting profiles in single section analyses may give a more accurate estimate of the relative frequency with which different targets are innervated than the registration of synapses. This is also indicated by the fact that even though their numbers are greater the intra- and interindividual differences in most categories evaluated in the quantitative studies were smaller for the CPs than for the SPs (Fig. 12b, c).

The variation of relative values was rather large in the categories CPs/SPs on dendritic shafts and on spines. A reason for this may be that in single section analyses of unusually thin sections, small dendritic shafts were mistaken for spines, since characteristic cytoplasmic features of dendrites were not included in the section. A possible explanation for the finding that in all nuclei the relative frequency of contacts on dendritic shafts as compared to contacts on spines shifts in favour of spines when synaptic contacts are compared may be that since the membrane area available for contacts is smaller in spines than it is in dendritic shafts, there is a greater chance of sectioning through the axospinous synapses in single section analysis than there is of sectioning through the axodendritic synapse.

TH-ir afferent fibres and their target neurons in the central nucleus

Comparison of the TH-ir innervation of the CeM and CeLcn yielded distinct features. The innervation density as measured by the number of TH-ir profiles in definite areas was higher in the CeLcn than in the CeM. This is consistent with recent light-microscopic investigations (Asan 1993; Freedman and Cassell 1994). Moreover, it showed that of the CeLcn TH-ir profiles a greater percentage forms synaptic contacts, leading to a synaptic density in the CeLcn more than twice as high as in the CeM.

The proportion of axospinous contacts in the CeLcn was higher than in the CeM. As mentioned above, about 18% of synaptic targets in the CeLcn could not be distinguished as small dendrites or spines. It is likely that many of these targets were actually spines, rendering the proportion of axospinous synapses in the CeLcn even higher.

Innervated neurons. Golgi and immunocytochemical studies have shown that the subdivisions of the CN contain morphologically and neurochemically differing neurons (McDonald 1982a; De Olmos et al. 1985; Cassell and Gray 1989). The majority of neurons in the CeM and fewer neurons in the CeLcn have been shown to project to brainstem centres such as the dorsal vagal and parabrachial nuclei or CA cell groups (e.g. Higgins and Schwaber 1983; Veening et al. 1984; Moga and Gray 1985; Cassell et al. 1986; Wallace et al. 1989; Gonzales and Chesselet 1990; Vankova et al. 1992; Sun and Cassell 1993; Sun et al. 1994). Since C1 neurons are by far the most frequent neurons of the CeM, it is likely that they are among the brainstem projection neurons. Our findings suggest that intense somatic TH-ir innervation is targeted at this neuron type. A major target of CeLcn projections is the bed nucleus of the stria terminals (Sun and Cassell 1993). The projection arises from medium-sized spiny neurons which constitute the predominant neuron type in the CeLcn (McDonald 1982a; Cassell and Gray 1989; Sun and Cassell 1993) and which are thought to additionally provide an intrinsic innervation of other CeLcn or of CeM neurons (Sun and Cassell 1993). Based on their relative frequency, it is likely that C3 and C4 neurons represent the ultrastructural counterpart of medium spiny CeLcn neurons. Again, some of these neurons receive abundant somatic TH-ir innervation. The occasionally encountered C1- and C2-type neurons could be the equivalent of the larger, moderately spiny and the medium-sized spine-sparse or aspinous neurons documented by Cassell and Gray (1989).

An interesting feature of the C3 and C4 neurons of the CeLcn is the close apposition of somata, with fused or thickened plasmalemmata and membranous vesicles in their vicinity. Similar phenomena have been described for neurotensin-ir and unlabelled CN neurons (Bayer et al. 1991) and for TH-ir and nonimmunoreactive neurons of the substantia nigra–ventral tegmental area (Bayer and Pickel 1990). Since in the latter neurons the presence of gap junctions has been suggested based on the fact that apposed neurons are electrically and dye coupled (for a review, see Bayer and Pickel 1990), the authors proposed that a similar coupling may exist between CeLcn neurons.

TH-ir afferent fibres and their target neurons in the basal complex

Light microscopy and quantitative evaluation of electron-microscopic preparations showed that the TH-ir innervation density of the BC was generally lower than that of the CN. In other respects, BC and CeM innervation characteristics such as preferential target structures and synaptic density were similar.

Innervated neurons. A comparison of our findings with those of Carlsen (1989) suggests that B1 neurons represent the principal projection neurons of the BC (McDonald 1982b; Carlsen and Heimer 1986, 1988). Several B1 neurons possessed intense somatic TH-ir innervation. Ultrastructural features indicate that B2 neurons are large and medium sized forms of class II neurons of McDonald (1982b; Carlsen 1989) and that B3 neurons represent small class II or possibly class III neurons (McDonald 1982b; Carlsen 1989). The latter two neuron types are supposedly local circuit neurons. Appositions of TH-ir axons were also found on B2 and B3 neurons, but synaptic specializations could not be ascertained.

TH-ir afferent fibres and their target neurons in the paracapsular intercalated cell groups

There is a profound difference between the TH-ir innervation pattern of the Ips and that found in the other amygdaloid nuclei. Even though the "normal"pattern of innervation of distal dendritic shafts and spines is also present, 20%–30% of the contacts, significantly more than in the other nuclei, are formed with proximal parts of the Ip neurons. Since at the borders of the small Ips the dendrites of Ip neurons are intermingled with those of the neighbouring lateral and BL neurons (Millhouse 1986), the proportion of proximal contacts may in effect be even higher than reported here.

Innervated neurons. The ultrastructure of rat I neurons has not been described yet. It has to be pointed out that we only looked at Ips. It is possible that the ultrastructure of neurons in the Im, which is dissimilar to the Ips in a number of characteristics (such as a significantly less dense DA innervation, see above), differs from that described here. However, Golgi studies (Millhouse 1986) indicate that the neuronal morphology is similar in all I cell groups, with medium spiny neurons constituting the largest population. The I1 neuron ultrastructure observed in our material is similar to that reported for I neurons in the cat in general (Paré and Smith 1993a). I2 neurons are likely to be the equivalent of the less frequent large neurons (Millhouse 1986; Paré and Smith 1993a). Many I1 neurons possess extensive somatosomatic contacts with each other. As in the CeLcn, there seem to be specialized zones in these appositions.

Functional considerations

Detection of different amygdaloid CA afferent fibres using the TH-immunoreaction. There are several lines of evidence suggesting that the TH-ir amygdaloid axons analysed in the present study represent predominantly DA afferent fibres. Thus, in accordance with previous studies (Gustafson and Greengard 1990; Asan 1993; Freedman and Cassell 1994), the CeLcn and the Ips possessed extremely dense TH-ir fibre plexus while being practically devoid of DBH- or PNMT-ir fibres. Therefore, the TH-ir axons in these nuclei represent almost exclusively DA afferent fibres.

The CeM and the BC receive a mixed CA innervation. In addition to the dense DA fibre plexus of these nuclei (Fallon et al. 1978; Fallon and Ciofi 1992; Freedman and Cassell 1994), NA projections from the locus coeruleus (LC) occur at a low density in the CeM and at a higher one in the BC (Fallon et al. 1978; Asan 1993) and are represented by the smooth type DBH-ir axons in the present study. NA and adrenergic (A) afferent fibres from the ventrolateral medullary CA cell groups are relatively frequent in the CeM and occasionally seen in the BM (Fallon et al. 1978; Hökfelt et al. 1984; Palkovits et al. 1992; Asan 1993, 1995). They are characterized by large varicosities as described here. In TH/DBH and TH/PNMT double labellings carried out on material which was fixed and immunocytochemically processed in the same way as in the present investigation, the TH immunoreaction failed to label NA projections from the LC (Asan 1993). This finding was substantiated in the present study by the observation that numerous DBH-ir fibres in the parietal cortex were not labelled in parallel TH-reacted sections. Since this cortical area receives a dense NA innervation from the LC (Moore and Bloom 1979) and the few TH-ir fibres found in layers II–V are likely to represent the sparse DA innervation encountered here (Descarries et al. 1987), the TH immunoreaction in the present material also did not detect NA projections from the LC. An explanation may be the lower concentration or detectability of TH in LC NA projections compared with DA axons documented in several previous studies in different species (Pickel et al. 1975; Schmidt and Bhatnagar 1979; Lewis et al. 1987; Milner and Bacon 1989; Sadikot and Parent 1990; Fallon and Ciofi 1992). Since ventrolateral medullary NA and A amygdala projections have been shown to contain a weak TH immunoreactivity (Asan 1993), some of the morphologically similar TH-ir type B axons documented in the present study may represent these CA afferent fibres. However, even in the CeM these axons constitute a very small population among all TH-ir structures. Thus, the description of the TH-ir afferent fibres in the present study reflects primarily DA innervation, and will be discussed below in relation to DA innervation in other brain areas.

1. Central nucleus. The arrangement of a TH-ir terminal forming a symmetric synapse on a spine or small dendrite which receives a neighbouring asymmetric synapse

from an unlabelled terminal, observed particularly in the CeLcn, is reminiscent of the arrangement of the DA innervation encountered in the neighbouring striatum (Freund et al. 1984). This innervation pattern suggests that the TH-ir afferent fibres, in line with their proposed striatal function, may regulate the selectivity of CeLcn neurons for stimuli reaching the nucleus from other sources (Freedman and Cassell 1994). Since the CN, in particular the CeLcn, is the target of cortical afferent fibres (Turner and Zimmer 1984; Kapp et al. 1985; McDonald and Jackson 1987; Sun et al. 1994) which terminate primarily upon small dendrites and dendritic spines (Sun et al. 1994), the TH-ir afferent fibres are in a position to modulate the effect of these inputs on the direct or indirect (via the BST or intrinsic connections, see above) output of the nucleus to brainstem centres involved in visceral, sensory or somatomotor processes (Higgins and Schwaber 1983; Veening et al. 1984; Moga and Gray 1985; Cassell et al. 1986; Wallace et al. 1989; Moga et al. 1989; Gonzales and Chesselet 1990; Vankova et al. 1992; Sun and Cassell 1993; Sun et al. 1994). This mode of action could help to explain the observed attenuating effect of DA injections into the CN on the development of stress-induced ulcers in rats (Ray et al. 1987).

The CeLcn is similar to the striatum also in a number of other respects, such as in the scarcity of NA or A innervation and in the presence of γ-aminobutyric acid (GABA) and enkephalin-synthesizing medium spiny neurons (Oertel et al. 1983). Moreover, the ultrastructure of striatal medium spiny neurons (Freund et al. 1984) resembles that of our C3 and C4 neurons. However, in the striatum, the proportion of spines contacted is higher than that of dendritic shafts (Freund et al. 1984), while in the CeLcn the situation is reversed. A possible reason for this could be the fact that dendrites of CeLcn medium spiny neurons are less spiny than their counterparts in the striatum (DeOlmos et al. 1985).

Additionally, a selected population of neurons in both CN subnuclei receives an intense perisomatic TH-ir input. Considering the high cell density especially in the CeLcn (McDonald 1982a), the absolute number of somatically contacted neurons may be quite high. An innervation of this type could exert a powerful nonselective influence on the activity of the contacted neuron. The functional significance of this type of TH-ir innervation remains to be determined.

2. Basal complex. The basolateral nucleus in the rat has been suggested to be organized like a cortical structure, based on similar neuronal morphology as well as comparable afferent and efferent innervation patterns (Carlsen and Heimer 1988; Carlsen 1989). In accordance with this proposition, the DA innervation observed in rat cortical areas (Séguéla et al. 1988; Verney et al. 1990) is similar to that of the TH-ir afferents in the BC. Thus, dendritic shafts are the preferential target structures, synapses are predominantly symmetric and most contacts form synapses (Séguéla et al. 1988). In contrast to the findings in the cortex, LGVs were generally not identifiable in BC TH-ir axons. While this may partly be due to the density of labelling in our material, we still feel that LGVs are generally rare in these axons.

Verney et al. (1990) propose that the cortical DA innervation is predominantly targeted at the dendritic tree of projection neurons, while interneurons are a minor target. Our findings are compatible with a similar arrangement of TH-ir terminals upon BC projection neurons. These neurons are the target of afferent fibres from cortical areas, the thalamus, the ventral forebrain cholinergic system and the lateral amygdaloid nucleus (Carlsen 1989; Stefanacci et al. 1991), which terminate primarily on the distal dendritic arbor. The afferent input effect is presumably susceptible to modulation by synapses formed by TH-ir terminals on more proximal parts of the dendritic tree.

As in the CN some neurons of the BC receive an intense proximal TH-ir innervation. While in the cortex appositions of DA afferent fibres with neuronal somata were observed (Séguéla et al. 1988; Verney et al. 1990), although synapses were not identified, B1 somata in the BC receive symmetric synapses from TH-ir terminals. A similar regional discrepancy has been noted in a study of the cholinergic innervation by Carlsen and Heimer (1986). These authors suggested that this could reflect a shift in input from soma to peripheral targets from phylogenetically older to younger areas.

The TH-ir innervation of the BC is thus in a position to control and gate the responsiveness of, for instance, BL neurons projecting to the nucleus accumbens (ACC; Kelley et al. 1982; Carlsen 1989) in response to extrinsic input. This manner of action may be a basis for effects observed after altering DA transmission in the BL–ACC connection, an important pathway in the expression of emotional behaviour (Louilot et al. 1985; Simon et al. 1988; Mogenson and Yim 1991; Scheel-Krüger and Willner 1991).

3. Paracapsular intercalated nuclei. Little is known about the connections of the Is. In his detailed Golgi study, Millhouse (1986) showed that Ip neurons extended axons toward the CN and M and collaterals into the BL. He further suggested that I neurons in general are interposed in projections from piriform and entorhinal cortices and the basal forebrain and lateral hypothalamus to the lateral, basal and central amygdaloid nuclei. Numerous reports agree that I1 neurons of all Is are GABAergic (Nitecka and Ben-Ari 1987; Paré and Smith 1993a; Pitkänen and Amaral 1994). Paré and Smith (1993a, b), showed that in the cat I neurons situated between the lateral, and basal nuclei and the central nucleus contribute a significant GABAergic input to the centromedial nuclei. They reported high spontaneous discharge rates of I neurons which they attributed to a lack of perisomatic GABAergic inhibition and suggested that the Is exert a tonic inhibitory influence over their projection targets. Assuming that the situation in the cat Is is similar to that in the densely DA innervated Ips in the rat, the intense somatic TH-ir input would be in an excellent position to directly influence the activity

of these I neurons including their inhibitory effect upon target neurons.

Concluding remarks

There appear to be three different TH-ir innervation patterns in the densely innervated amygdaloid nuclei: (1) the presumably modulatory "cortical-like" input, most likely directed at projection neurons in the BC and similarly encountered in the CeM; (2) the intense, "striatal-like" innervation which presumably modulates the activity of CeLcn neurons in response to extrinsic input; and (3) the less-selective proximal innervation of the Ips. Thus, the TH-ir innervation – representing, as demonstrated, predominantly DA afferent fibres – is undoubtedly in a position to exert significant influence on the intrinsic organization and the extensive output of the rat amygdala. The features described here for the rat may be relevant also for higher vertebrates, since the studied nuclei in the rat and the equivalent nuclei in the primate exhibit a high degree of similarity in cyto- and chemoarchitectonics and with respect to connectional characteristics (e.g. Price et al. 1987; Amaral et al. 1992). Also, at the LM level, the TH-ir innervation in the monkey (Sadikot and Parent 1990) is similar to that in the rat.

In all species studied, including the human, the nuclei investigated are either part of or heavily project to a basal forebrain entity consisting of the CN, the BST, the dorsal substantia innominata and possibly the medial ACC, which is called the "central extended amygdala" (Alheid and Heimer 1988; DeOlmos 1990; Alheid et al. 1995). This complex is considered to control and gate the ascending and descending output of the limbic system (Alheid and Heimer 1988; Scheel-Krüger and Willner 1991), and is thus involved in all aspects of functions ascribed to the amygdala, including emotional behaviour, social communication and attentional and memory processes. In man, dysfuntion of information processing in the complex may play a crucial role in the etiology of psychoses. Alterations in the systems modulating this information processing may well be the cause of some psychotic abnormalities. For instance, a loss of DA modulation in the amygdala could be relevant for the occurrence of anxiety disorders frequently observed in patients suffering from Parkinson's disease (Stein et al. 1990). Also, the extended amygdala is a likely target of psychotherapeutic drugs acting through their effect on DA receptors (Alheid and Heimer 1988). The present results are a step towards understanding how CA innervation, in this case predominantly the DA afferent fibres, act in the amygdala of the rat. Given the similarities in the organization of the central extended amygdala between lower and higher vertebrates (see above), the findings may eventually help to uncover the effect of dysfunctions in these systems in humans.

Acknowledgements. The author wishes to thank H. Wiener, M. Rupp and T. Manger-Harasim for their excellent technical assistance and Prof. A. Wree for supplying GA-fixed brains.

References

Adolphs R, Tranel D, Damasio H, Damasio A (1994) Impaired recognition of emotion in facial expressions following bilateral damage to the human amygdala. Nature 372:669–672

Alheid GF, Heimer L (1988) New perspectives in basal forebrain organization of special relevance for neuropsychiatric disorders. The striatopallidal, amygdaloid, and corticopetal components of substantia innominata. Neuroscience 27:1–39

Alheid GF, DeOlmos JS, Beltramino CA (1995) Amygdala and extended amygdala. In: Paxinos G (ed) The rat nervous system, 2nd edition. Academic Press, San Diego, pp 495–578

Allman J, Brothers L (1994) Faces, fear and the amygdala. Nature 372:613–614

Amaral DG, Price JL, Pitkänen A, Charmichael ST (1992) Anatomical organization of the primate amygdaloid complex. In: Aggleton JP (ed) The amygdala. Neurobiological aspects of emotion, memory, and mental dysfunction. Wiley-Liss, New York, pp 1–66

Asan E (1993) Comparative single and double immunolabelling with antisera against catecholamine biosynthetic enzymes: criteria for the identification of dopaminergic, noradrenergic and adrenergic structures in selected rat brain areas. Histochemistry 99:427–442

Asan E (1995) The adrenergic innervation of the rat central amygdaloid nucleus: a light and electron microscopic study using phenylethanolamine N-methyltransferase as a marker. Anat Embryol (Berl) 192:471–481

Bayer VE, Pickel VM (1990) Ultrastructural localization of tyrosine hydroxylase in the rat ventral tegmental area: relationship between immunolabeling density and neuronal associations. J Neurosci 10:2996–3013

Bayer VE, Towle AC, Pickel VM (1991) Vesicular and cytoplasmic localization of neurotensin-like immunoreactivity (NTLI) in neurons postsynaptic to terminals containing NTLI and/or tyrosine hydroxylase in the rat central nucleus of the amygdala. J Neurosci Res 30:398–413

Berod A, Hartman BK, Pujol JF (1981) Importance of fixation in immunohistochemistry: use of formaldehyde solutions at variable pH for the localization of tyrosine hydroxylase. J Histochem Cytochem 29:844–850

Carlsen J (1988) Immunocytochemical localization of glutamate decarboxylase in the rat basolateral amygdaloid nucleus, with special reference to GABAergic innervation of amygdalostriatal projection neurons. J Comp Neurol 2173:513–526

Carlsen J (1989) New perspectives on the functional anatomical organization of the basolateral amygdala. Acta Neurol Scand 79 [Suppl] 122:1–28

Carlsen J, Heimer L (1986) A correlated light and electron microscopic immunocytochemical study of cholinergic terminals and neurons in the rat amygdaloid body with special emphasis on the basolateral amygdaloid nucleus. J Comp Neurol 244:121–136

Carlsen J, Heimer L (1988) The basolateral amygdaloid complex as a cortical-like structure. Brain Res 441:377–380

Cassell MD, Gray TS (1989) Morphology of peptide-immunoreactive neurons in the rat central nucleus of the amygdala. J Comp Neurol 281:320–333

Cassell MD, Gray TS, Kiss JZ (1986) Neuronal architecture in the rat central nucleus of the amygdala: a cytological, hodological, and immunocytochemical study. J Comp Neurol 246:478–499

DeOlmos J (1990) Amygdala. In: Paxinos G (ed) The human nervous system. Academic Press, San Diego, pp 583–710

DeOlmos J, Alheid GF, Beltramino C (1985) Amygdala. In: Paxinos G (ed) The rat nervous system. Academic Press, Australia, pp 223–334

Descarries L, Lemay B, Doucet G, Berger B (1987) Regional and laminar density of the dopamine innervation in adult rat cerebral cortex. Neuroscience 21:807–824

Erselius RT, Wree A (1991) Ultrastructure of axons in stereotaxically placed ibotenic acid-induced lesions of the hippocampus in the adult rat. Evidence for demyelination and degeneration of dispersed axons of passage. J Hirnforsch 32:139–148

Fallon JH, Ciofi P (1992) Distribution of monoamines within the amygdala. In: Aggleton JP (ed) The Amygdala. Neurobiological aspects of emotion, memory, and mental dysfunction. Wiley-Liss, New York, pp 97–114

Fallon JH, Koziell DA, Moore RY (1978) Catecholamine innervation of the basal forebrain II. Amygdala, suprarhinal cortex and entorhinal cortex. J Comp Neurol 180:509–531

Fibiger HC (1991) The dopamine hypotheses of schizophrenia and mood disorders: contradictions and speculations. In: Willner P, Scheel-Krüger J (eds) The mesolimbic dopamine system: from motivation to action. Wiley, Chichester, pp 615–637

Freedman LJ, Cassell MD (1994) Distribution of dopaminergic fibers in the central division of the extended amygdala of the rat. Brain Res 633:243–252

Freund TF, Powell JF, Smith AD (1984) Tyrosine hydroxylase-immunoreactive boutons in synaptic contact with identified striatonigral neurons, with particular reference to dendritic spines. Neuroscience 13:1189–1215

Gallagher M, Holland PC (1994) The amygdala complex: multiple roles in associative learning and attention. Proc Natl Acad Sci USA 91:11771–11776

Glavin GB, Murison R, Overmier JB, Pare WP, Bakke HK, Henke PG, Hernandez DE (1991) The neurobiology of stress ulcers. Brain Res Rev 16:301–343

Gonzales C, Chesselet MF (1990) Amygdalonigral pathway: an anterograde study in the rat with *Phaseolus vulgaris* leucoagglutinin (PHA-L). J Comp Neurol 297:182–200

Gustafson EL, Greengard P (1990) Localization of DARPP-32 immunoreactive neurons in the bed nucleus of the stria terminalis and central nucleus of the amygdala: co-distribution with axons containing tyrosine hydroxylase, vasoactive intestinal polypeptide, and calcitonin gene-related peptide. Exp Brain Res 79:447–458

Higgins GA, Schwaber JS (1983) Somatostatinergic projections from the central nucleus of the amygdala to the vagal nuclei. Peptides 4:657–662

Hökfelt T, Johansson O, Goldstein M (1984) Central catecholamine neurons as revealed by immunohistochemistry with special reference to adrenaline neurones. In: Björklund A, Hökfelt T (eds) Handbook of chemical neuroanatomy, vol 2, part 1. Elsevier, Amsterdam, pp 157–276

Kapp BS, Schwaber JS, Driscoll PA (1985) The organization of insular cortex projections to the amygdaloid central nucleus and autonomic regulatory nuclei of the dorsal medulla. Brain Res 360:355–360

Kelley AE, Domesick VB, Nauta WJH (1982) The amygdalostriatal projection in the rat – an anatomical study by anterograde and retrograde tracting methods. Neuroscience 7:615–630

Kilts CD, Anderson CM, Ely TD, Mailman RB (1988) The biochemistry and pharmacology of mesoamygdaloid dopamine neurons. Ann NY Acad Sci 537:173–187

LeDoux JE (1994) Emotion, memory and the brain. Sci Am 1994:32–39

Lewis DA, Campbell MJ, Foote SL, Goldstein M, Morrison JH (1987) The distribution of tyrosine hydroxylase-immunoreactive fibers in primate neocortex is widespread but regionally specific. J Neurosci 7:279–290

Liposits Z, Sherman D, Phelix C, Paul WK (1986) A combined light and electron microscopic immunocytochemical method for the simultaneous localization of multiple tissue antigens. Histochemistry 85:95–106

Louilot A, Simon H, Taghzouti K, LeMoal M (1985) Modulation of dopaminergic activity in the nucleus accumbens following facilitation or blockade of the dopaminergic transmission in the amygdala: a study by in vivo differential pulse voltammetry. Brain Res 346:141–145

McDonald AJ (1982a) Cytoarchitecture of the central amygdaloid nucleus of the rat. J Comp Neurol 208:401–418

McDonald AJ (1982b) Neurons of the lateral and basolateral amygdaloid nuclei: a Golgi study in the rat. J Comp Neurol 212:293–312

McDonald AJ, Jackson TR (1987) Amygdaloid connections with posterior insular and temporal cortical areas in the rat. J Comp Neurol 262:59–77

Millhouse OE (1986) The intercalated cells of the amygdala. J Comp Neurol 247:246–271

Milner TA, Bacon CE (1989) Ultrastructural localization of tyrosine hydroxylase-like immunoreactivity in the rat hippocampal formation. J Comp Neurol 281:479–495

Moga MM, Gray TS (1985) Evidence for corticotropin-releasing factor, neurotensin, and somatostatin in the neural pathway from the central nucleus of the amygdala to the parabrachial nucleus. J Comp Neurol 241:275–284

Moga MM, Saper CB, Gray TS (1989) Bed nucleus of the stria terminalis: cytoarchitecture, immunohistochemistry, and projection to the parabrachial nucleus in the rat. J Comp Neurol 283:315–322

Mogenson GJ, Yim CC (1991) Neuromodulatory function of the mesolimbic dopamine system: electrophysiological and behavioural studies. In: Willner P, Scheel-Krüger J (eds) The mesolimbic dopamine system: from motivation to action. Wiley, Chichester, pp 105–130

Moore RY, Bloom FE (1979) Central catecholamine neuron systems: anatomy and physiology of the norepinephrine and epinephrine systems. Annu Rev Neurosci 2:113–168

Nitecka L, Ben-Ari Y (1987) Distribution of GABA-like immunoreactivity in the rat amygdaloid complex. J Comp Neurol 266:45–55

Oertel WH, Riethmüller G, Mugnaini E, Schmechel DE, Windl A, Gramsch C, Herz A (1983) Opioid peptide-like immunoreactivity localized in GABAergic neurons of rat neostriatum and central amygdaloid nucleus. Life Sci 33 [Suppl I]:73–76

Palkovits M, Mezey E, Skirboli LR, Hökfelt T (1992) Adrenergic projections from the lower brainstem to the hypothalamic paraventricular nucleus, the lateral hypothalamic area and the central nucleus of the amygdala in rats. J Chem Neuroanat 5:407–415

Paré D, Smith Y (1993a) Distribution of GABA immunoreactivity in the amygdaloid complex of the cat. Neuroscience 57:1061–1076

Paré D, Smith Y (1993b) The intercalated cell masses project to the central and medial nuclei of the amygdala in cats. Neuroscience 57:1077–1090

Paxinos G, Watson C (1986) The rat brain in stereotaxic coordinates. Academic Press, Sydney

Peters A, Palay SL, Webster de F (1991) The fine structure of the nervous system, 3rd edition. Oxford University Press, New York

Pickel VM, Joh TH, Field PM, Becker CG, Reis DJ (1975) Cellular localization of tyrosine hydroxylase by immunohistochemistry. J Histochem Cytochem 23:1–12

Pitkänen A, Amaral DG (1994) The distribution of GABAergic cells, fibers and terminals in the monkey amygdaloid complex: an immunohistochemical and in situ hybridization study. J Neurosci 14:2200–2224

Price JL, Russchen FT, Amaral DG (1987) The limbic region. II. The amygdaloid complex. In: Björklund A, Hökfelt T, Swanson LW (eds) Handbook of chemical neuroanatomy, vol 5. Integrated systems of the CNS, part 1. Elsevier, Amsterdam

Ray A, Henke PG, Sullivan RM (1987) The central amygdala and immobilization stress-induced gastric pathology in rats: neurotensin and dopamine. Brain Res 409:398–402

Reynolds GP (1963) The use of lead citrate at high pH as an electron-opaque stain in electron microscopy. J Cell Biol 17:208–212

Sadikot AF, Parent A (1990) The monoaminergic innervation of the amygdala in the squirrel monkey: an immunohistochemical study. Neuroscience 36:431–447

Scheel-Krüger J, Willner P (1991) The mesolimbic system: principles of operation. In: Willner P, Scheel-Krüger J (eds) The mesolimbic dopamine system: from motivation to action. Wiley and Sons, Chichester, pp 559–597

Schmidt RH, Bhatnagar RK (1979) Assessment of the effects of neonatal subcutaneous 6-hydroxydopamine on noradrenergic and dopaminergic innervation of the cerebral cortex. Brain Res 166:309–319

Séguéla P, Watkins KC, Descarries L (1988) Ultrastructural features of dopamine axon terminals in the anteromedial and the suprarhinal cortex of adult rat. Brain Res 442:11–22

Simon J, Taghzouti K, Gozlan H, Studler JM, Louilot A, Herve D, Glowinski J, Tassin JP, LeMoal M (1988) Lesion of dopaminergic terminals in the amygdala produces enhanced locomotor response to D-amphetamine and opposite changes in dopaminergic activity in prefrontal cortex and nucleus accumbens. Brain Res 447:335–340

Stefanacci L, Farb CR, Pitkänen A, Go G, LeDoux JE, Amaral DG (1991) Projections from the lateral nucleus to the basal nucleus of the amygdala: a light and electron microscopic PHA-L study in the rat. J Comp Neurol 323:586–601

Stein MB, Heuser IJ, Juncos JL, Uhde TW (1990) Anxiety disorders in patients with Parkinson's disease. Am J Psychiatry 147:217–220

Sun N, Cassell MD (1993) Intrinsic GABAergic neurons in the rat central extended amygdala. J Comp Neurol 330:381–404

Sun N, Yi H, Cassell MD (1994) Evidence for a GABAergic interface between cortical afferents and brainstem projection neurons in the rat central extended amygdala. J Comp Neurol 340:43–64

Tovée MJ (1995) What are faces for? Curr Biol 5:480–482

Turner BH, Zimmer J (1984) The architecture and some of the interconnections of the rat's amygdala and lateral periallocortex. J Comp Neurol 227:540–557

Vankova M, Arluison M, Leviel V, Tramu G (1992) Afferent connections of the rat substantia nigra pars lateralis with special reference to peptide-containing neurons of the amygdalo–nigral pathway. J Chem Neuroanat 5:39–50

Veening JG, Swanson LW, Sawchenko PE (1984) The organization of projections from the central nucleus of the amygdala to brainstem sites involved in central autonomic regulation: a combined retrograde transport–immunohistochemical study. Brain Res 308:337–357

Verney C, Alvarez C, Geffard M, Berger B (1990) Ultrastructural double-labelling study of dopamine terminals and GABA-containing neurons in rat anteromedial cerebral cortex. Eur J Neurosci 2:960–972

Wallace DM, Magnuson DJ, Gray TS (1989) The amygdalo-brainstem pathway: selective innervation of dopaminergic, noradrenergic and adrenergic cells in the rat. Neurosci Lett 97:252–258

Zaborsky L, Heimer L (1989) Combinations of tracer techniques, especially HRP and PHA-L, with transmitter identification for correlated light and electron microscopic studies. In: Heimer L, Zaborsky L (eds) Neuroanatomical tract tracing methods 2. Plenum Press, New York, pp 49–96